eNeuro

Research Article: New Research | Development

Impaired interneuron development in a novel model of neonatal brain injury

Helene Lacaille, PhD[1], Claire-Marie Vacher, PhD[1], Dana Bakalar, PhD[1], Jiaqi J. O'Reilly, M.Phil[1,2], Jacquelyn Salzbank, M.Ed[1] and Anna A Penn, MD, PhD[1,2,3]

[1]*Center for Neuroscience, Children's Natl. Hlth. Syst., Washington, DC*
[2]*Institute for Biomedical Sciences, George Washington University, Washington, DC*
[3]*Fetal Med. Institute, Neonatology, Children's Natl. Hlth. Syst, Washington, DC*

https://doi.org/10.1523/ENEURO.0300-18.2019

Received: 1 August 2018

Revised: 27 December 2018

Accepted: 3 January 2019

Published: 31 January 2019

Author contributions: HL, CMV and AAP designed the study. HL conducted experiments and acquired data. HL and AAP analyzed and interpreted the data and wrote the paper. HL, CMV, DB, JJOR, JS and AAP interpreted the data and edited the paper. AAP supervised the project.

Funding: NIH NICHD
R01HD092593
U54 HD090257

Funding: Cerebral Palsy Alliance Research Foundation
PG1914

Funding: Children's national health system
44290

Funding: Children's national board of visitors
44392

Funding: Children's research institute
1181

Conflict of Interest: The authors report no conflict of interest.

Correspondence should be addressed to Anna Penn, apenn@childrensnational.org

Cite as: eNeuro 2019; 10.1523/ENEURO.0300-18.2019

Impaired interneuron development in a novel model of neonatal brain injury

Abbreviated title: Altered interneuron development in preterm birth

Helene Lacaille, PhD[1], Claire-Marie Vacher, PhD[1], Dana Bakalar, PhD[1], Jiaqi J. O'Reilly, M.Phil[1,2], Jacquelyn Salzbank, M.Ed[1], Anna A Penn, MD, PhD[1,2,3]

[1] Center for Neuroscience, Children's Natl. Hlth. Syst., Washington, DC
[2] Institute for Biomedical Sciences, George Washington University, Washington, DC
[3] Fetal Med. Institute, Neonatology, Children's Natl. Hlth. Syst, Washington, DC

HL, CMV and AAP designed the study. HL conducted experiments and acquired data. HL and AAP analyzed and interpreted the data and wrote the paper. HL, CMV, DB, JJOR, JS and AAP interpreted the data and edited the paper. AAP supervised the project.

Corresponding author: Anna Penn, MD, PhD, Fetal & Transitional Medicine, Neonatology, Center for Neuroscience Research, Children's National Health System
111 Michigan Avenue, NW, Washington, DC 20010, USA
Phone: +1 202-476-4324, Fax: +1 202-476-4988
apenn@childrensnational.org

Number of figures: 7

Number of tables: 3

Number of multimedia: 0

Number of words for Abstract: 256

Number of words for Significance Statement: 114

Number of words for Introduction: 803

Number of words for Discussion: 1543

Acknowledgements

We thank Drs J. Scafidi and L. Wang for neurobehavioral equipment and testing assistance. We thank Eresha Bluth and Janine Burgess for expert assistance. We thank Drs V. Gallo and M. Shoykhet for their constructive criticism of the manuscript. We gratefully acknowledge the contribution of families to the NIH Neurobiobank, as well as J. Cottrell (NIH Neurobiobank) who assisted us throughout the process of human tissue selection.

Conflict of interest: The authors report no conflict of interest

Funding sources

Supported by NIH R01HD092593, District of Columbia Intellectual Developmental Disabilities Research Center U54HD090257, Cerebral Palsy Alliance Research Foundation, Children's National Health System, Children's National Board of Visitors, Children's Research Institute and Fetal Medicine Institute, Washington DC.

Abstract

Prematurity is associated with significantly increased risk of neurobehavioral pathologies, including autism and schizophrenia. A common feature of these psychiatric disorders is prefrontal cortex (PFC) inhibitory circuit disruption due to GABAergic interneuron alteration. Cortical interneurons are generated and migrate throughout late gestation and early infancy, making them highly susceptible to perinatal insults such as preterm birth. Term and preterm PFC pathology specimens were assessed using immunohistochemical markers for interneurons. Based on the changes seen, a new preterm encephalopathy mouse model was developed to produce similar PFC interneuron loss. Maternal immune activation (MIA; modeling chorioamnionitis, associated with 85% of extremely preterm births) was combined with chronic sublethal hypoxia (CSH; modeling preterm respiratory failure), with offspring of both sexes assessed anatomically, molecularly and neurobehaviorally. In the PFC examined from the human preterm samples compared to matched term samples at corrected age, a decrease in somatostatin and calbindin interneurons was seen in upper cortical layers. This pattern of interneuron loss in upper cortical layers was mimicked in the mouse PFC following the combination of MIA and CSH, but not after either insult alone. This persistent interneuron loss is associated with postnatal microglial activation that occurs during CSH only after MIA. The combined insults lead to long-term neurobehavioral deficits which parallel human psychopathologies that may be seen after extremely preterm birth. This new preclinical model supports a paradigm in which specific cellular alterations seen in preterm encephalopathy can be linked with a risk of neuropsychiatric sequela. Specific interneuron subtypes may provide therapeutic targets to prevent or ameliorate these neurodevelopmental risks.

Significance Statement

Growing evidence suggests that a common component of psychiatric disorders is damage to inhibitory neurons. In the frontal lobe, these neurons continue to develop during late gestation and infancy, predisposing preterm survivors to neurobehavioral disorders and/or cognitive impairment. Preventing neuronal damage depends on having accurate models of preterm brain injury with well-defined outcome measures that can be examined in both small animals and humans. In this study, interneuron number were assessed in term and preterm human frontal brain tissues and in a novel multifactorial model that combines prenatal inflammation with postnatal hypoxia resulting in long-term inhibitory neuron loss. This new model was validated through anatomical and functional assessments that directly translate to human measures.

Introduction

Dysfunction of the prefrontal cortex (PFC) underlies a number of deficits associated with psychiatric disorders, particularly their cognitive and social components(Sugranyes et al., 2011). A common feature of these psychiatric disorders is a disruption of PFC inhibitory circuits, mediated by developmental alterations of Gamma-Aminobutyric Acid (GABA) interneurons(Marin, 2012). Interneuron loss, misplacement, and dysmaturation characterize these disorders(Gogolla et al., 2009; Meechan et al., 2009; Takano, 2015; Filice et al., 2016; Hashemi et al., 2017). Specifically, GABAergic network alteration in the Brodmann area 9 (BA9; dorsolateral PFC), a region involved in working memory and social cognition, may account for specific cognitive deficits of these disorders(Tooney and Chahl, 2004; Samaco et al., 2005; Fatemi et al., 2009; Habl et al., 2012; Hashemi et al., 2017).

GABA progenitor cells proliferate in the fetal brain (at least through 35 weeks of gestation)(Arshad et al., 2016) and then migrate to the frontal lobes and mature during infancy(Paredes et al., 2016), leaving these interneurons precursors highly susceptible to perinatal insults. A correlation between prematurity, GABA concentration and abnormal functional connectivity has been demonstrated in the BA9(Kwon et al., 2014), raising the possibility that alterations in interneuron number or function may contribute to increase the risk of later neurodevelopmental psychopathology associated with preterm birth (Johnson and Marlow, 2011).

Preterm birth (delivery prior to 37 weeks of gestation) is a multifactorial syndrome. Chorioamnionitis occurs in up to 85% of extremely preterm births and is strongly associated with an increased risk of spontaneous preterm delivery(Blencowe et al., 2013). After preterm birth, additional insults such as respiratory failure can increase

the risk of long-term impairments, including disorders of executive functioning, autism and schizophrenia(Adams-Chapman and Stoll, 2006; Arpino et al., 2010; Meldrum et al., 2013; Knuesel et al., 2014; Lombardo et al., 2017).

Understanding interneuron alterations after preterm birth can contribute to a better comprehension of the perinatal environment's impact on psychiatric disorders. In this study, examination of a set of human preterm and term post-mortem samples have demonstrated decreased density of specific PFC interneuron subpopulations. To investigate this finding of persistent interneuron loss, a novel multi-insult mouse model was then developed, using both prenatal maternal immune activation (MIA) and postnatal chronic sublethal hypoxia (CSH), designed to capture the type and timing of common perinatal physiological insults. Prior models have induced early MIA resulting in limited deficits of cortical interneurons(Carpentier et al., 2013; Canetta et al., 2016). Likewise, postnatal insults during the first 2 weeks of rodent life, such as hypoxia-ischemia or chronic sublethal hypoxia (CSH), have been used to mimic white matter abnormalities that develop in preterm infants (Mayoral et al., 2009; Salmaso et al., 2014; Scafidi et al., 2014; Zonouzi et al., 2015). Limited alterations of interneuron numbers (Fagel et al., 2009) or delayed interneuron maturation (Komitova et al., 2013) have been described after these postnatal insults, but these changes do not recapitulate the human pathology depicted here. Rather, unlike embryonic MIA or postnatal CSH alone, the combination of insults significantly disrupts the density of mature interneurons in the PFC - mimicking the cellular alterations seen in the samples from extremely preterm neonates examined here- and induces specific cognitive deficits.

This multi-hit protocol is proposed as a novel preclinical model to decipher the cellular and physiological mechanisms underlying the deficits seen in preterm survivors

exposed to inflammation and hypoxia that may make them vulnerable to later neuropsychiatric disorders.

Methods and Materials

Study approval

All animal procedures were performed in accordance with the with the Children's National Institutional Animal Care and Use Committee (#00030312).

Human Samples

Human samples were obtained from the NIH Neurobiobank at University of Maryland, Baltimore, MD (ID #709). Donors consisted of corrected age preterm and matched term infants, excluding those with major congenital anomalies, or known genetic diagnoses and those with meningitis or stroke as cause of death. Sex, gestational weeks, absolute age (postnatal age) and corrected age are shown in Table 1. Brodmann Area9 (BA9) formalin-fixed brain samples were cut into 0.5-cm-thick coronal slices and preserved in 10% neutral buffered formalin; matched frozen tissues were preserved at -80C.

Animals

Experimental mice were produced by a heterozygous breeding scheme in which GAD65-GFP transgenics (C57BL/6 background) (obtained from Dr. Vittorio Gallo, generated from Dr. Gabor Szabo(Lopez-Bendito et al., 2004)) were crossed to C57BL/6 mice. For time pregnant mating, male and female pairs were housed overnight, with the following day designated as embryonic day (E) 0.5. The day of birth was designated as postnatal day (P) 0. For all experiments described here, embryos and postnatal pups of both sexes were included. Each experimental group contained pups from at least two litters.

Maternal Immune Activation and Chronic Sublethal Hypoxia

Mild, late MIA was induced using 150 µg/kg of Lipopolysaccharide (LPS; L6529, from Escherichia coli O55:B5, MilliporeSigma, Burlington, MA, USA), administered to the pregnant dam intraperitoneally on both E15.5 and 16.5. After delivery, dams and litters were housed in 10.9% oxygen from P3 to P10 to produce CSH, with control litters housed in the same room outside of the hypoxia chamber. No adverse effects of hypoxia were noted on dams or pups, except for mild growth restriction that resolved over the first postnatal month (Salmaso et al., 2015). Four experimental groups were studied: mice treated with saline and reared under normoxia (MIA-/CSH-), mice subjected to MIA and reared under normoxia (MIA+/CSH-), mice treated with saline and reared under CSH (MIA-/CSH+) and mice subjected to MIA and reared under CSH (MIA+/CSH+). Mice from multiple litters were randomly assigned to these groups and groups were balanced for litter size and sex.

Immunohistochemical procedure

Human tissue: Formalin-fixed tissues were cryoprotected in a 30% sucrose solution and embedded in Tissue-Tek® O.C.T. Compound (Sakura® Finetek, Torrance, CA, USA). Blocks were cut into 25-µm-thick sections on a cryostat and mounted on Superfrost Plus (ThermoFisher, Waltham, MA, USA) glass slides. Frozen sections were allowed to equilibrate to room temperature for 2 hours before staining.

Mouse tissue: Embryonic brains were obtained after euthanasia of the dam by CO_2 asphyxiation followed by cerebral dislocation; brains were quickly dissected in 1X Phosphate Buffered Saline (PBS) and transferred to 4% paraformaldehyde (PFA). Postnatal mice were perfused at P10 or P30 with 1X PBS/4% PFA and brains were

post-fixed in 4% PFA for 24h and transferred into 30% sucrose in 1X PBS. Brains were sectioned into coronal 40-µm thick sections with a sliding microtome before immunolabeling.

Procedure: Tissue sections were rinsed in PBS-Triton 0.3% (PBS-T) then blocked in PBS-T with 10% normal donkey serum (NDS) followed by overnight incubation at 4°C in PBS-T-10% NDS with primary antibodies: BrdU (1:500, Abcam, Cambridge, MA, USA, ab6326), Calbindin (1:1000, Swant Marly, Switzerland, Cb300 or Cb38), Calretinin (1/1000, MilliporeSigma AB1550), cleaved-Caspase-3 (1:500, Cell Signaling Technology, Danvers, MA, USA, Asp175), CD68 (1:300, Bio-Rad, Hercules, CA, USA, MCA1957GA), Gad65-67 (1/200 Santa Cruz Biotechnology sc-365180), Gad67 (1/100, MilliporeSigma MAB5406), GFP (1/500, Abcam, Ab13970), Iba1 (1:500, Wako Chemicals, Richmond VA, USA, 019-19741), Ki67 (1/500, Abcam, ab15580), NeuN (1/500, Abcam, ab177487), Neuropetide Y (1:500, Immunostar, Hudson, WI, USA, 22940), Parvalbumin (1/1000, MilliporeSigma, P3088), Somatostatin (1:300, Santa Cruz Biotechnology, Santa Cruz, CA, USA, sc7819), Reelin (1:300, R&D systems, Minneapolis, MN, USA, AF3820), VIP (1:1000, Immunostar, 20077). For secondary detection, appropriately matched Alexa Fluor-conjugated secondary antibodies (1:500, ThermoFisher) were incubated 90 min in PBS-T at room temperature. For all groups studied, dividing cells were detected with bromodeoxyuridine (BrdU, Roche, Manheim, Germany) injected at E15.5 intraperitoneally at 50 mg/kg. For BrdU staining, a pre-DNA denaturation step was performed by incubating the sections in 2N HCl for 30 min at 45°C before the primary antibody incubation. Sections were incubated with DAPI, mounted in Fluoromount G (ThermoFisher) and coverslipped before confocal examination (Olympus FV1000, Center Valley PA, USA).

Quantification: For human sections, the cell density was assessed in the upper layers (UL), lower layers (LL) and the subcortical white matter (SWM) of BA9 and expressed in cells per mm^2. Cortical layering was determined with DAPI counterstaining. For mouse tissues, results from four sections per animal and five to six animals per group were average and the number of cells in each cortical sub-region was expressed as density of cells per mm^3. Cortical layering was determined with DAPI counterstaining(Skorput et al., 2015); The delineation between the anterior cingulate cortex (ACC) and the prelimbic area (PL) is based on the Allen Brain Atlas. Cell quantification was performed using the Imaris-Bitplane software (South Windsor, CT, USA). All counts were performed blind to condition.

Real-Time PCR (RT-PCR)

Human tissue: BA9 tissues were homogenized in TRIzol™ Reagent (ThermoFisher, 15596018); total RNA was extracted with the RNeasy Mini Kit (Qiagen Venlo, Netherlands, 74104).

Mouse tissue: Cerebral cortices were collected in RNA later (Qiagen, 76106); total RNA was extracted with the PARIS™ Kit (ThermoFisher, AM1921) and quantified with a Nanodrop ND-2000C (ThermoFisher).

Procedure: 1 µg of RNA was used to make cDNA with the iScript cDNA Synthesis Kit (Bio-Rad, 1708891). All primer pairs were designed and validated in-house for efficiency and specificity. RT-PCR experiments were performed on cDNA samples in presence of SsoAdvanced Universal SYBR Green Supermix (Bio-Rad, 1725271) with specific primers at 100nM using the ABI Prism 7500 Sequence Detection System ThermoFisher). The cDNA-generated signals for target genes were internally corrected

with transferrin receptor protein 1 (*tfrc*) for human tissues and phosphoglycerate kinase 1 (*pgk1*) for mouse tissues. The regulation was determined with the $2^{-\Delta\Delta Cq}$ method.

Western Blot

Human samples were homogenized in RIPA lysis buffer with proteinase inhibitors (Santa Cruz Biotechnology, sc24948). Protein extracts, 40 µg per lane, were loaded onto 4–20% gradient gels (NuSep Inc Germantown, MD, USA, NB10-420). Gels were electrotransfered to a 0.2 µm nitrocellulose membrane (Bio-Rad, 1620174). Blots were blocked in 5% milk in TBST for 1 h, and then incubated at 4 °C overnight with one of the following antibodies: anti-gad65; -gad67; -somatostatin; -gapdh (Santa Cruz Biotechnology, sc377145, sc28376, sc7819, sc32233) -calbindin (Swant Marly, Cb38), and -calretinin (MilliporeSigma, AB1550). Bands were detected with appropriate horseradish peroxide-conjugated secondary antibodies, reacted with chemiluminescent ECL substrate (Bio-Rad, 1705060) and visualized with a BioRad ChemiDoc Imaging system. Band intensity was measured using the ImageJ program (NIH).

Behavioral experiments

Testing began at P30 and a 1-week inter-test interval was provided between each test paradigm.

Barnes maze investigation and reinvestigation: The Barnes maze (Stoelting Co, Wood Dale, IL, USA) consisted of a circular disk with equally spaced holes. The number and position of nose-pokes over a 10-min period were recorded for each animal. Repeated pokes into previously explored holes were divided by the number of initial pokes.

Y-maze spontaneous alternation: Mice were placed in a Y-shaped maze. The number of arm entries over a 10-min period was recorded. The alternation index was calculated as the number of total complete alternations, divided by the total number of arm entries minus two and expressed as a percentage.

Water T-maze and reversal learning: Testing occurred in a 6-cm deep T-maze (Stoelting Co, Wood Dale, IL) filled with water (22°C ± 1). A clear platform 10 mm under the water surface was placed at the end of the left or right arms. On days 1 to 5, animals were trained to locate the hidden platform with 4 trials per day. On day 6, the platform location was switched to the opposite arm of the T-maze and training continued until day 9.

Socialization test: Testing occurred in a 3-chamber box (Stoelting Co). The two outer compartments contained metal wire cages where stranger mice 1 and 2 (S1 and S2) were held. After 10-min of habituation, the test animal was placed in the middle chamber with the adjacent doors closed. S1 was placed in one cage and an object (O) in the other. The doors were opened to allow the test animal 10 min exploration. Social interaction duration (test mouse nose in contact with cage containing S1) was measured. S2 subsequently replaced the O and the test mouse was allowed another 10 minutes exploration. The time spent with either S1 or S2 was divided by the time spent with S1+O for social preference, or S1+S2 for novelty, and expressed as percentage.

Open Field: Anxiety and activity were examined in an Open Field (40 cm x 40 cm; Stoelting). Mice were recorded and analyzed over 10 min with ANY-maze (Stoelting). Tracing paths of the mice were recorded and time spent in the central part (25 cm x 25 cm) versus time spent at the border was evaluated.

Marble burying: This test for repetitive behavior was performed in a box filled with 5 cm of bedding. Twelve glass marbles were evenly placed on the surface of the bedding. The number of buried marbles (to 2/3 of their depth) was counted after a 30-min exploration period.

Statistics

All experiments and analysis were performed blind to conditions. Statistical analysis was performed using PRISM software (GraphPad Software 6.0, San Diego, CA, USA). Normal distribution of each dataset was analyzed by Shapiro-Wilk test. When two conditions were compared, data were analyzed with a nonparametric Mann-Whitney test. When four experimental groups were assessed, and three conditions compared to the control group, data were analyzed with a one-way ANOVA with Holm-Sidak's multiple comparisons or Kruskal–Wallis with Dunn's multiple comparisons. When four experimental groups were assessed and two variables were taken into consideration, data were analyzed with a two-way ANOVA with Fisher LSD, Sidak's or Tukey's multiple comparisons. In Figure 2, the statistical analysis was performed layer by layer with a Kruskal–Wallis with Dunn's multiple comparisons. The null hypothesis was rejected for alpha greater than 5%. The Statistical analysis is reported in detail in Table 2.

Results

Major subtypes of interneurons are decreased in the human preterm PFC

The PFC, including Brodmann area 9 (BA9), is one of the brain regions most frequently altered in psychiatric disease. To address whether interneuron density in this region was altered by prematurity, BA9 sections from 13 term and 14 preterm infants were obtained. Mean age of death (absolute age) was 1.5 months in term infants and 3.7 months for preterm infants delivered between 26 and 34 weeks of gestation (average corrected age 1.1 months). Sex, gestational weeks and cause of death varied, but none were attributed to CNS infection, hemorrhage or malformation (Table 1). Genetic diseases or anatomical birth defects were excluded.

Interneuron subtypes express specific molecular markers, in addition to expressing markers for GABA synthesis (GAD65 and GAD67). These subtypes have distinct morphologies, connectivity and physiology that allow precise inhibitory control of local neural networks(Tremblay et al., 2016). Some types can be identified by non-overlapping marker expression (somatostatin (SST), parvalbumin (PV), and sets of vasoactive intestinal peptide (VIP) expressing and non-expressing interneurons) while other molecular markers are expressed in populations that overlap with the major markers (calretinin (CRT), calbindin (CLB), or neuropeptide Y (NPY). Major subclasses of interneurons were assessed by immunostaining for GAD65-67, SST, CLB, CRT and NPY to detect the major types of human interneurons for which antibodies are available (in male Figure 1 and female Figure 1-1, term and preterm infants). Interneurons were counted in 3 sub-regions of BA9; the upper layers (UL), lower layers (LL) and the subcortical white matter (SWM).

A trend toward decrease was observed in the BA9 of human preterm male infants for GAD65-67$^+$ (UL -24% ns, LL -16% ns, SWM +17%, ns Figure 1A-A') and a significant reduction in the number of SST$^+$ (UL -31% P<0.05, LL -2% ns, SWM +1%, ns Figure 1B-B') and CLB$^+$ (UL -28% P<0.05, LL +15% ns, SWM +9%, ns Figure 1C-C') interneurons in upper but not lower layers. CRT$^+$ interneurons density was increased in the SWM (UL -17% ns, LL +9% ns, SWM +63%, P<0.05 Figure 1D-D'). No change was observed in the number of NPY$^+$ interneurons (Figure 1E-E'). PV$^+$ was not detected in this set of human samples, although these cells could be detected at later developmental stages (data not shown). No statistically significant change in total cortical layer widths was discernable based on Nissl staining (data not shown), suggesting overall preservation of pyramidal cells at this age. No difference was observed in female infants, but statistical power was limited by the small sample size (Figure 1-1). Global interneuron-related protein expression was not altered in the BA9 of preterm infants (Figure 1-2), however interneuron-related transcripts for *gad2* and *calb1* were increased (Figure 1-3).

The multi-hit model alters interneurons density and distribution

To develop a new preclinical model that captures the multiple insults of human preterm brain injury, as well as the specific interneuron loss observed in the human samples studied here, prenatal MIA, induced by low dose LPS given late in gestation was combined with postnatal CSH induced by housing in a hypoxic environment for a week. Four experimental groups were used: mice whose dams were treated with saline and reared under normoxia (MIA-/CSH-); mice whose dams were treated with LPS and reared under normoxia (MIA+/CSH-); those treated with saline and reared in hypoxia

(MIA-/CSH+); and those treated with LPS and reared in hypoxia (MIA+/CSH+; the "multi-hit" model).

Total interneuron density, illustrated in Figure 2 A-D, was analyzed by counting cells positive for GAD65 in the two main sub-regions of the PFC, the anterior cingulate cortex (ACC, Figure 2A'-B') and prelimbic area (PL, Figure 2A''-B''). Density and laminar distribution were analyzed and both $GAD65^+$ (-36% $P<0.05$, Figure 2A'; -33% $P<0.05$, Figure 2A'') and $GAD67^+$ (-22% $P<0.05$, Figure 2B'; -23% $P<0.05$, Figure 2B'') were significantly decreased in the MIA+/CSH+ cohort at P30. The multi-hit model also induced a long-lasting decrease in the density of SST^+ (-32% $P<0.05$, Figure 2C'; -57% $P<0.05$, Figure 2C'') and CLB^+ (-22% $P<0.05$, Figure 2D'; -57% $P<0.05$, Figure 2D''), similar to the findings in human preterm PFC. In this animal model, no sex differences were detected so sexes were combined in further analyses.

Five additional subtypes of interneuron present in the PFC of mice were analyzed: PV (Figure 2-1A), VIP (Figure 2-1B), CRT (Figure 2-1C), NPY (Figure 2-1D), and reelin (RLN; Figure 2-1E). All subtypes except RLN were reduced. Only PV^+ (-32% $P<0.05$, Figure 2-1A'; -60% $P<0.05$, Figure 2-1A'') and SST^+ (Figure 2C-C''), both in layer II/III, were exclusively decreased after both hits. Similarly, MIA altered the density and distribution of VIP^+, in ACC layer V (MIA+/CSH- -70% $P<0.05$; MIA+/CSH+ -31% $P<0.05$, Figure 2-1B') and PL layer II/III (MIA+/CSH- -43% $P<0.05$, MIA+/CSH+ -41% $P<0.05$, Figure 2-1B''). CSH alone led to a reduction in CLB^+ in layer V that was similar to the multi-hit model (MIA-/CSH+ -42% $P<0.05$, MIA+/CSH+ -22% $P<0.05$, Figure 2-D'; MIA-/CSH+ -38% $P<0.05$, MIA+/CSH+ -57% $P<0.05$, Figure 2-D''). In contrast CRT^+ and NPY^+ subtypes were decreased after either MIA or CSH, as well as by the combination of insults (Figure 2-1C and 2-1D). Taken together, these data point out

unique changes induced in the multi-hit model in GAD65, GAD67, PV, and SST expressing interneurons.

PFC interneuron loss due to MIA-induced alteration of proliferation and migration plus CSH-induced maturation delay

To understand the mechanisms underlying the alterations induced by the multi-hit model in the PFC, the direct effect of mild late inflammation was examined at E17.5. Comparing fetuses from MIA versus saline exposed gestations revealed a significant decrease in the number of GAD65-GFP$^+$ in 3 major sub-divisions of the developing cerebral cortex (MZ -36%, CP -33%, SVZ/VZ -25% $P<0.05$, Figure 3A-A'). To elucidate the cause of interneuron loss, Ki67 (a marker of mitosis) was used in combination with GAD65 to label interneuron progenitors proliferation in the caudal ganglionic eminence (CGE), one of the 3 germinative areas where the majority of GAD65$^+$ interneurons are generated. At E17.5, MIA significantly reduced Ki67$^+$, and cells double-labeled for GAD65$^+$ and Ki67$^+$ (-32% $P<0.05$, Figure 3B''; -43% $P<0.01$, Figure 3B*). Interneuron density in the medial ganglionic eminence (MGE) and preoptic area was determined by Nkx2.1 expression, a marker of interneuron progenitors. Like GAD65$^+$, Nkx2.1$^+$ cell density did not differ in these germinative zones but was significantly decreased in embryonic cortex (-35% $P<0.05$, Figure 3-1).

To assess the contribution of survival and migration to the loss of cortical interneurons, MIA and saline control dams were injected at E15.5 with BrdU, which labels actively dividing cells during a restricted period (Fig3C). At E17.5, MIA exposure significantly decreased BrdU$^+$ GAD65$^+$ double-labelled cells in the PFC (-72% $P<0.01$, Figure 3C*). The contribution of apoptotic cell death to the loss of cortical interneurons

was examined, but no significant difference was observed in cleaved caspase 3-positive cells (Figure 3-2). A small decrease in neuronal density was observed using NeuN$^+$ (Figure 3-3), but this reduction was significantly less than the percentage of GAD65$^+$ neurons lost. Overall, these data highlight alterations of interneuron proliferation and suggest an alteration of migration induced by MIA.

To examine the molecular factors involved in interneuron loss, the expression of 18 interneuron-related transcripts was assessed at E17.5 in the cerebral cortex of mice subjected to MIA or saline. A significant increase was observed in the expression of fate determination (*gad2*, +57%; *nkx2.1*, +142%; *lhx6*, +92%; *ki67*, +62%, Table 3) and migration mRNAs (*dlx1*, +51%; dlx5, +176%, Table 3) suggesting that early interneuron suppression may lead to a compensatory increases in genes that can promote subsequent interneuron progenitor production.

The addition of postnatal hypoxia was then assessed (Figure 4). In MIA+/CSH- mice, GAD65$^+$ cell numbers recovered by P10. This recovery was abolished by addition of CSH (MIA+/CSH- -8% ns, MIA+/CSH+ -49% $P<0.05$, Figure 4A'). With hypoxia treatment alone (MIA-/CSH+), fewer GAD65$^+$ cells were also seen, suggesting a direct effect of hypoxia on interneuron survival which was confirmed by co-labeling GAD65 with BrdU (injected at E15.5; Figure 4A''). MIA+/CSH+ cortex at P30 showed long-lasting interneuron deficits (Figure 4B-B''). Overall, MIA induced an early loss of interneurons through proliferation and migration defects which, with the addition of CSH, prevented recovery so that these deficits persisted into adulthood (MIA+/CSH+ E17.5 -44% $P<0.001$, P10 -49% $P<0.05$, P30 -37% $P<0.05$, Figure 5).

The addition of CSH induced a second burst of inflammation

To determine the effect of the multi-hit model on inflammation, the density of Iba1 positive cells was used to determine the total number of microglia and $Iba1^+$ $CD68^+$ double-labeled cells detected microglial activation. At E17.5, microglial numbers (+22% $P<0.05$, Figure 6A') and microglial activation (+75% $P<0.01$, Figure 6A'') were increased by MIA. By P10, only MIA+/CSH+ significantly increased activated microglia (MIA+/CSH- +61%, ns; MIA-/CSH+ +34%, ns; MIA+/CSH+ +135%, $P<0.01$, Figure 6B'') suggesting a sensitization of microglial cells by MIA to a second inflammatory response induced by hypoxia. These inflammatory markers had declined by P30 although interneuron loss persisted (Figure 6C-C'').

The multi-hit model alters working memory, cognitive flexibility and social cognition

To further define long-term behavioral alterations potentially linked to PFC GABAergic network deficits, neurobehavioral tests for working memory, cognitive flexibility and social cognition were performed.

Working memory was analyzed through the spontaneous alternation task in the Y-maze, where the alternation level was significantly lower in mice exposed to MIA+/CSH+, and similar in mice exposed to MIA only (MIA+/CSH- -13%, ns; MIA+/CSH+ -20% $P<0.001$, Figure 7A). This working memory deficit was confirmed in the Barnes maze test where the repeated investigation of previously explored holes was significantly higher in MIA+/CSH+ animals (+47% $P<0.01$, Figure 7B), while the number of arm entries and nose-pokes remained stable across groups (Figure 7-1A-B).

Cognitive flexibility was examined using the reversal-learning task of the water T-maze. No difference was observed for learning the initial location of the platform (Figure

392 7C). In contrast, during the reversal learning phase, MIA+/CSH+ mice required more
393 time to learn the new location, with lower performance on day 2 and 3 (day 2 -35%,
394 $P<0.05$, day 3 -59% $P<0.05$, Figure 7D). No significant difference was observed
395 between groups by day 4 (Figure 7D).

396 Social cognition was evaluated with social preference and novelty in the 3-
397 chamber test. During social preference, all the groups spent more than 70% of the time
398 with the conspecific animal (Figure 7E). A similar pattern was observed during social
399 novelty testing, where groups spent more time with the unfamiliar mouse (Figure 7F).
400 However, even though MIA+/CSH+ mice discriminate between the unfamiliar and
401 familiar animal, they spent significantly less time interacting with the unfamiliar animal
402 compared to controls (-12% $P<0.05$, Figure 7F) and exhibited decreased total
403 interaction time (-26% $P<0.05$, Figure 7G). No significant difference was observed for
404 activity and anxiety in the open-field (Figure 7-1C-E) or for repetitive behavior with the
405 marble burying test (Figure 7-1F).

406 Overall, this new multi-hit mouse model decreases several subtypes of
407 interneurons in the upper layers of the PFC and induces behavioral deficits
408 characteristic of schizophrenia-like disorders. The observation of a pronounced
409 decrease in the density of multiple interneuron subtypes in the human preterm brain
410 samples examined here suggests that alterations of interneurons following extreme
411 prematurity might be a risk factor for psychiatric disorders or other neurodevelopmental
412 disabilities that can follow preterm birth.

413

Discussion

Elucidating the effects of perinatal insults on GABAergic interneuron development is critical to understand the mechanistic role they play in the pathogenesis of neuropsychiatric disorders. While human glutamatergic neurogenesis is complete by 28 weeks of gestation(Malik et al., 2013), GABAergic progenitors persist in the ganglionic eminences through at least 35 weeks of gestation and continue to migrate into the cortex throughout the perinatal period (Sanai et al., 2011; Arshad et al., 2016; Paredes et al., 2016), suggesting that perinatal insults may be significant environmental factors predisposing preterm survivors to psychiatric disorders.

In the present study, the BA9 of 1-month old term and 1-month term corrected-age very preterm infants were compared. A decrease in the density of both SST and CLB interneuron subtypes was seen in the upper layers of the frontal cortex from these preterm infants. Human pathology studies remain limited, but our findings are consistent with prior studies showing altered interneuron expression in preterm infants (aged from a few hours to a few weeks postpartum) in the white matter and subplate(Robinson et al., 2006), and in the cortical plate(Panda et al., 2018).

The human tissue used here comes from preterm donors who survived up to 5 months and were subjected to the adverse environment of prematurity for a significant period. While the insults that lead directly to death may have contributed to our findings, the immediate cause of death was similar in both the preterm and term infants (most commonly “sudden infant death syndrome”, while confounding genetic or obviously infectious diagnoses were excluded). However, the possibility remains that the observed PFC interneuron deficit may be linked not only to chorioamnionitis and respiratory compromise but to a variety of perinatal insults, many of which remain

438 undefined. Human data suggest that generation of interneurons well into the postnatal
439 period (Yang et al., 2011; Arshad et al., 2016; Paredes et al., 2016) raising the
440 possibility that human survivors of extreme prematurity could subsequently produce
441 interneurons to compensate for the observed loss. Many preterm infants survive
442 neurologically intact and this post-mortem sampling may reflect a more compromised
443 population or a delay in interneuron development that would have recovered. In the
444 future, non-invasive methods that measure localized GABA concentrations in living
445 infants may help clarify these issues, but such techniques do not yet have the resolution
446 required, so models must be used to better understand the progression of injury and
447 underlying mechanisms.

448 Pairing two previously established methods (MIA and CSH) created a novel
449 model of preterm encephalopathy that more closely mimics this human pathology.
450 Unlike other multi-hit models(Jantzie et al., 2014; Mallard and Vexler, 2015), the use of
451 MIA and CSH spans both pre- and postnatal periods, which is more representative of
452 when preterm encephalopathy develops. Preclinical models of preterm brain injury are
453 most successful when using multifactorial approaches that account for the complexity of
454 the perinatal environment (Elovitz and Mrinalini, 2004; Manuel et al., 2017). The multi-
455 hit mouse model was designed to investigate the effects of perinatal insults associated
456 with preterm birth, producing a model in which later neurobehavioral disorders could be
457 assessed.

458 Density of both GAD65 and GAD67 expressing cells was reduced, consistent
459 with prior reports of prematurity-related decreases in *gad1* and *gad2* transcripts,
460 encoding GAD67 and GAD65, in the PFC (Richetto et al., 2014; Labouesse et al.,
461 2015). The decrease observed here was specific to layer II/III. In mice, cortical

462 interneurons are generated in the MGE between E9.5 and E15.5 with a peak at E12.5,
463 contributing to the cortical layers in an inside-out manner(Butt et al., 2007), and from the
464 CGE between E12.5 and E18.5, with a peak at E16.5, contributing to the superficial
465 layers(Miyoshi et al., 2007; Miyoshi et al., 2010; Torigoe et al., 2016). This data
466 suggests that MIA altered the proliferation and migration of interneurons from the late
467 MGE or from the CGE. A prior transcriptomic study using MIA shown down-regulation of
468 transcripts involved in interneuron tangential migration including the Distal-less (*Dlx*)
469 family and both GAD isoforms(Oskvig et al., 2012), suggesting that impaired migration
470 may also play a role in the findings observed in E17.5 cortex. Prenatal stress has also
471 been shown to reduce the distribution of interneurons by impairing their
472 migration(Stevens et al., 2013).

473 While PV neurons are known to be selectively altered by MIA(Canetta et al.,
474 2016), the other interneuron subtypes have been less comprehensively studied in the
475 context of perinatal brain injury. In mouse PFC, a reduced density and laminar
476 distribution of PV is observed, as well as decreased numbers of SST, CLB, VIP, CRT
477 and NPY after combined MIA plus CSH. This is the first demonstration of decreased
478 density of CLB, CRT and NPY in a model of perinatal brain injury. A delay in maturation
479 of these neurons may explain these effects, as suggested by a study in which hypoxia
480 induced a decrease in PV, SST and VIP immunoreactivity that partially recovered at
481 later stages(Komitova et al., 2013). The data from the ganglionic eminences suggest
482 decreased interneurogenesis following MIA, followed by possible maturation defects as
483 a consequence of postnatal CSH, supporting a combination of alterations on
484 interneuron development.

MIA produces an early alteration of interneurogenesis followed by possible maturation defects as a consequence of postnatal CSH, but the underlying mechanisms by which maternal inflammation or postnatal hypoxia perturbs brain development remain unknown. Blocking the actions of specific cytokines such as IL-1β prevents MIA-induced behavioral and physiological consequences in mouse offspring, suggesting a role for pro-inflammatory cytokines in the process(Girard et al., 2010). In support of this, in the multi-hit model, a transient activation of microglial cells is showed after MIA, which is significantly enhanced by later CSH. These findings, along with a recent report in a different mixed model(Zhou et al., 2017), highlight the extension of MIA-induced inflammatory response by CSH, suggesting that postnatal insults potentiate abnormalities caused by *in utero* inflammation to permanently alter brain development.

To further define long-term behavioral alterations potentially linked to GABAergic network deficits in the PFC, a battery of neurobehavioral tests was performed. The multi-hit model of preterm brain injury induced deficits in working memory, cognitive flexibility and social interaction. Direct alterations of excitatory and inhibitory balance within the PFC have a strong effect on social motivation, predominantly mediated by PV and SST interneuron subtypes(Bicks et al., 2015), potentially underlying the deficits seen in social novelty and social interaction.

Alterations in working memory have been extensively discussed in the context of psychiatric disorders. MIA, a known cause of such disorders, has been shown to impair working memory in offspring(Murray et al., 2017). Additionally, specific lesion of PV neurons in the PFC produces deficits in working memory and cognitive flexibility(Murray et al., 2015). Involvement of SST interneurons has also been demonstrated, although PV and SST interneurons show distinct contributions to PFC circuit dynamics underlying

working memory(Kim et al., 2016). Impaired working memory in the multi-hit model may be associated with reduced GABAergic transmission by PV and SST interneurons in the adult PFC, but further investigations are needed to directly link specific interneuron losses with the observed behavioral phenotypes. Interestingly, lesion of the PFC or complete disruption of $GABA_A$-receptor-mediated inhibition in the PFC by bicuculline infusion has been shown to recapitulate the behavioral deficits induced by the multi-hit model(Auger and Floresco, 2014; Hernan et al., 2014; Murray et al., 2015) supporting the hypothesis that the observed interneuron loss could cause the measured behavioral deficits.

In contrast to prior studies, here MIA alone did not impair working memory. This difference may stem from uses of lower LPS doses or timing of administration(Meyer et al., 2008). On the other hand, perinatal hypoxia alone induces impairments in associative learning, spatial memory, and long-term social memory that have been linked with white matter deficits(Cengiz et al., 2011; Lan et al., 2011; Salmaso et al., 2012). White matter injury has been mechanistically linked to interneuron deficits because interneurons promote oligodendrocytes development (Voronova et al., 2017), with hypoxic interneuron loss potentially contributing to impaired myelination.

Abnormalities in cortical interneurons have been broadly associated with cognitive deficits in the context of psychiatric disorders. The reduction of multiple interneuron subtypes in this model is consistent with prior observations in patients with schizophrenia. This pathology is also commonly cited with changes in GABA system-related transcripts, with altered expression of GABA-synthesizing enzymes, (GAD65 and GAD67), GABA transporter systems and interneuron markers (SST, NPY, CLB, RLN and cholecystokinin) reported(Hashimoto et al., 2003; Hashimoto et al., 2008b;

Hashimoto et al., 2008a; Maldonado-Aviles et al., 2009; Mellios et al., 2009; Volk et al., 2012). In this model, the potentiation of inflammation by postnatal CSH may increase the risk of psychiatric-related neurobehavioral deficits by producing latent inflammation with microglial activation across a critical developmental time(Meyer et al., 2011). Whether other more subtle indicators of latent inflammation persist into adulthood after the microglial activation subsides, as has been suggested for human autism spectrum disorders and schizophrenia(Meyer et al., 2011), remains to be explored. While the mechanistic links between loss of specific PFC interneurons and specific psychiatric deficits in both mouse and human need to be further investigated, the observed deficits are consistent with the cognitive (working memory and cognitive flexibility) and negative symptoms (social dysfunction) of schizophrenia. Thus, this model provides new opportunities to interrogate the molecular mechanisms that link perinatal insults, interneuron deficits and later neuropsychiatric risk.

References

Adams-Chapman I, Stoll BJ (2006) Neonatal infection and long-term neurodevelopmental outcome in the preterm infant. Curr Opin Infect Dis 19:290-297.

Arpino C, Compagnone E, Montanaro ML, Cacciatore D, De Luca A, Cerulli A, Di Girolamo S, Curatolo P (2010) Preterm birth and neurodevelopmental outcome: a review. Childs Nerv Syst 26:1139-1149.

Arshad A, Vose LR, Vinukonda G, Hu F, Yoshikawa K, Csiszar A, Brumberg JC, Ballabh P (2016) Extended Production of Cortical Interneurons into the Third Trimester of Human Gestation. Cereb Cortex 26:2242-2256.

Auger ML, Floresco SB (2014) Prefrontal cortical GABA modulation of spatial reference and working memory. Int J Neuropsychopharmacol 18.

Bicks LK, Koike H, Akbarian S, Morishita H (2015) Prefrontal Cortex and Social Cognition in Mouse and Man. Front Psychol 6:1805.

Blencowe H, Cousens S, Chou D, Oestergaard M, Say L, Moller AB, Kinney M, Lawn J (2013) Born too soon: the global epidemiology of 15 million preterm births. Reprod Health 10 Suppl 1:S2.

Butt SJ, Cobos I, Golden J, Kessaris N, Pachnis V, Anderson S (2007) Transcriptional regulation of cortical interneuron development. The Journal of neuroscience : the official journal of the Society for Neuroscience 27:11847-11850.

Canetta S, Bolkan S, Padilla-Coreano N, Song LJ, Sahn R, Harrison NL, Gordon JA, Brown A, Kellendonk C (2016) Maternal immune activation leads to selective functional deficits in offspring parvalbumin interneurons. Mol Psychiatry 21:956-968.

571 Carpentier PA, Haditsch U, Braun AE, Cantu AV, Moon HM, Price RO, Anderson MP,
572 Saravanapandian V, Ismail K, Rivera M, Weimann JM, Palmer TD (2013)
573 Stereotypical alterations in cortical patterning are associated with maternal
574 illness-induced placental dysfunction. The Journal of neuroscience : the official
575 journal of the Society for Neuroscience 33:16874-16888.
576 Cengiz P, Uluc K, Kendigelen P, Akture E, Hutchinson E, Song C, Zhang L, Lee J,
577 Budoff GE, Meyerand E, Sun D, Ferrazzano P (2011) Chronic neurological
578 deficits in mice after perinatal hypoxia and ischemia correlate with hemispheric
579 tissue loss and white matter injury detected by MRI. Dev Neurosci 33:270-279.
580 Elovitz MA, Mrinalini C (2004) Animal models of preterm birth. Trends Endocrinol Metab
581 15:479-487.
582 Fagel DM, Ganat Y, Cheng E, Silbereis J, Ohkubo Y, Ment LR, Vaccarino FM (2009)
583 Fgfr1 is required for cortical regeneration and repair after perinatal hypoxia. The
584 Journal of neuroscience : the official journal of the Society for Neuroscience
585 29:1202-1211.
586 Fatemi SH, Reutiman TJ, Folsom TD, Thuras PD (2009) GABA(A) receptor
587 downregulation in brains of subjects with autism. J Autism Dev Disord 39:223-
588 230.
589 Filice F, Vorckel KJ, Sungur AO, Wohr M, Schwaller B (2016) Reduction in parvalbumin
590 expression not loss of the parvalbumin-expressing GABA interneuron
591 subpopulation in genetic parvalbumin and shank mouse models of autism. Mol
592 Brain 9:10.

593 Girard S, Tremblay L, Lepage M, Sebire G (2010) IL-1 receptor antagonist protects
594 against placental and neurodevelopmental defects induced by maternal
595 inflammation. J Immunol 184:3997-4005.
596 Gogolla N, Leblanc JJ, Quast KB, Sudhof TC, Fagiolini M, Hensch TK (2009) Common
597 circuit defect of excitatory-inhibitory balance in mouse models of autism. J
598 Neurodev Disord 1:172-181.
599 Habl G, Schmitt A, Zink M, von Wilmsdorff M, Yeganeh-Doost P, Jatzko A, Schneider-
600 Axmann T, Bauer M, Falkai P (2012) Decreased reelin expression in the left
601 prefrontal cortex (BA9) in chronic schizophrenia patients. Neuropsychobiology
602 66:57-62.
603 Hashemi E, Ariza J, Rogers H, Noctor SC, Martinez-Cerdeno V (2017) The Number of
604 Parvalbumin-Expressing Interneurons Is Decreased in the Medial Prefrontal
605 Cortex in Autism. Cereb Cortex 27:1931-1943.
606 Hashimoto T, Bazmi HH, Mirnics K, Wu Q, Sampson AR, Lewis DA (2008a) Conserved
607 regional patterns of GABA-related transcript expression in the neocortex of
608 subjects with schizophrenia. Am J Psychiatry 165:479-489.
609 Hashimoto T, Volk DW, Eggan SM, Mirnics K, Pierri JN, Sun Z, Sampson AR, Lewis DA
610 (2003) Gene expression deficits in a subclass of GABA neurons in the prefrontal
611 cortex of subjects with schizophrenia. The Journal of neuroscience : the official
612 journal of the Society for Neuroscience 23:6315-6326.
613 Hashimoto T, Arion D, Unger T, Maldonado-Aviles JG, Morris HM, Volk DW, Mirnics K,
614 Lewis DA (2008b) Alterations in GABA-related transcriptome in the dorsolateral
615 prefrontal cortex of subjects with schizophrenia. Mol Psychiatry 13:147-161.

616 Hernan AE, Alexander A, Jenks KR, Barry J, Lenck-Santini PP, Isaeva E, Holmes GL,
617 Scott RC (2014) Focal epileptiform activity in the prefrontal cortex is associated
618 with long-term attention and sociability deficits. Neurobiol Dis 63:25-34.
619 Jantzie LL, Corbett CJ, Berglass J, Firl DJ, Flores J, Mannix R, Robinson S (2014)
620 Complex pattern of interaction between in utero hypoxia-ischemia and intra-
621 amniotic inflammation disrupts brain development and motor function. J
622 Neuroinflammation 11:131.
623 Johnson S, Marlow N (2011) Preterm birth and childhood psychiatric disorders. Pediatr
624 Res 69:11r-18r.
625 Kim D, Jeong H, Lee J, Ghim JW, Her ES, Lee SH, Jung MW (2016) Distinct Roles of
626 Parvalbumin- and Somatostatin-Expressing Interneurons in Working Memory.
627 Neuron 92:902-915.
628 Knuesel I, Chicha L, Britschgi M, Schobel SA, Bodmer M, Hellings JA, Toovey S,
629 Prinssen EP (2014) Maternal immune activation and abnormal brain
630 development across CNS disorders. Nat Rev Neurol 10:643-660.
631 Komitova M, Xenos D, Salmaso N, Tran KM, Brand T, Schwartz ML, Ment L, Vaccarino
632 FM (2013) Hypoxia-induced developmental delays of inhibitory interneurons are
633 reversed by environmental enrichment in the postnatal mouse forebrain. The
634 Journal of neuroscience : the official journal of the Society for Neuroscience
635 33:13375-13387.
636 Kwon SH, Scheinost D, Lacadie C, Benjamin J, Myers EH, Qiu M, Schneider KC,
637 Rothman DL, Constable RT, Ment LR (2014) GABA, resting-state connectivity
638 and the developing brain. Neonatology 106:149-155.

639 Labouesse MA, Dong E, Grayson DR, Guidotti A, Meyer U (2015) Maternal immune
640 activation induces GAD1 and GAD2 promoter remodeling in the offspring
641 prefrontal cortex. Epigenetics 10:1143-1155.
642 Lan WC, Priestley M, Mayoral SR, Tian L, Shamloo M, Penn AA (2011) Sex-specific
643 cognitive deficits and regional brain volume loss in mice exposed to chronic,
644 sublethal hypoxia. Pediatr Res 70:15-20.
645 Lombardo MV, Moon HM, Su J, Palmer TD, Courchesne E, Pramparo T (2017)
646 Maternal immune activation dysregulation of the fetal brain transcriptome and
647 relevance to the pathophysiology of autism spectrum disorder. Mol Psychiatry.
648 Lopez-Bendito G, Sturgess K, Erdelyi F, Szabo G, Molnar Z, Paulsen O (2004)
649 Preferential origin and layer destination of GAD65-GFP cortical interneurons.
650 Cereb Cortex 14:1122-1133.
651 Maldonado-Aviles JG, Curley AA, Hashimoto T, Morrow AL, Ramsey AJ, O'Donnell P,
652 Volk DW, Lewis DA (2009) Altered markers of tonic inhibition in the dorsolateral
653 prefrontal cortex of subjects with schizophrenia. Am J Psychiatry 166:450-459.
654 Malik S, Vinukonda G, Vose LR, Diamond D, Bhimavarapu BB, Hu F, Zia MT, Hevner
655 R, Zecevic N, Ballabh P (2013) Neurogenesis continues in the third trimester of
656 pregnancy and is suppressed by premature birth. The Journal of neuroscience :
657 the official journal of the Society for Neuroscience 33:411-423.
658 Mallard C, Vexler ZS (2015) Modeling Ischemia in the Immature Brain: How
659 Translational Are Animal Models? Stroke 46:3006-3011.
660 Manuel CR, Ashby CR, Reznik SE (2017) Discrepancies in Animal Models of Preterm
661 Birth. Curr Pharm Des.

662 Marin O (2012) Interneuron dysfunction in psychiatric disorders. Nat Rev Neurosci
663 13:107-120.
664 Mayoral SR, Omar G, Penn AA (2009) Sex differences in a hypoxia model of preterm
665 brain damage. Pediatr Res 66:248-253.
666 Meechan DW, Tucker ES, Maynard TM, LaMantia AS (2009) Diminished dosage of
667 22q11 genes disrupts neurogenesis and cortical development in a mouse model
668 of 22q11 deletion/DiGeorge syndrome. Proc Natl Acad Sci U S A 106:16434-
669 16445.
670 Meldrum SJ, Strunk T, Currie A, Prescott SL, Simmer K, Whitehouse AJ (2013) Autism
671 spectrum disorder in children born preterm-role of exposure to perinatal
672 inflammation. Front Neurosci 7:123.
673 Mellios N, Huang HS, Baker SP, Galdzicka M, Ginns E, Akbarian S (2009) Molecular
674 determinants of dysregulated GABAergic gene expression in the prefrontal cortex
675 of subjects with schizophrenia. Biol Psychiatry 65:1006-1014.
676 Meyer U, Feldon J, Dammann O (2011) Schizophrenia and autism: both shared and
677 disorder-specific pathogenesis via perinatal inflammation? Pediatr Res 69:26r-
678 33r.
679 Meyer U, Nyffeler M, Yee BK, Knuesel I, Feldon J (2008) Adult brain and behavioral
680 pathological markers of prenatal immune challenge during early/middle and late
681 fetal development in mice. Brain Behav Immun 22:469-486.
682 Miyoshi G, Butt SJ, Takebayashi H, Fishell G (2007) Physiologically distinct temporal
683 cohorts of cortical interneurons arise from telencephalic Olig2-expressing
684 precursors. The Journal of neuroscience : the official journal of the Society for
685 Neuroscience 27:7786-7798.

686 Miyoshi G, Hjerling-Leffler J, Karayannis T, Sousa VH, Butt SJ, Battiste J, Johnson JE,
687 Machold RP, Fishell G (2010) Genetic fate mapping reveals that the caudal
688 ganglionic eminence produces a large and diverse population of superficial
689 cortical interneurons. The Journal of neuroscience : the official journal of the
690 Society for Neuroscience 30:1582-1594.
691 Murray AJ, Woloszynowska-Fraser MU, Ansel-Bollepalli L, Cole KL, Foggetti A, Crouch
692 B, Riedel G, Wulff P (2015) Parvalbumin-positive interneurons of the prefrontal
693 cortex support working memory and cognitive flexibility. Sci Rep 5:16778.
694 Murray BG, Davies DA, Molder JJ, Howland JG (2017) Maternal immune activation
695 during pregnancy in rats impairs working memory capacity of the offspring.
696 Neurobiol Learn Mem 141:150-156.
697 Oskvig DB, Elkahloun AG, Johnson KR, Phillips TM, Herkenham M (2012) Maternal
698 immune activation by LPS selectively alters specific gene expression profiles of
699 interneuron migration and oxidative stress in the fetus without triggering a fetal
700 immune response. Brain Behav Immun 26:623-634.
701 Panda S, Dohare P, Jain S, Parikh N, Singla P, Mehdizadeh R, Klebe DW, Kleinman
702 GM, Cheng B, Ballabh P (2018) Estrogen Treatment Reverses Prematurity-
703 Induced Disruption in Cortical Interneuron Population. The Journal of
704 neuroscience : the official journal of the Society for Neuroscience 38:7378-7391.
705 Paredes MF, James D, Gil-Perotin S, Kim H, Cotter JA, Ng C, Sandoval K, Rowitch DH,
706 Xu D, McQuillen PS, Garcia-Verdugo JM, Huang EJ, Alvarez-Buylla A (2016)
707 Extensive migration of young neurons into the infant human frontal lobe. Science
708 354.

709 Richetto J, Calabrese F, Riva MA, Meyer U (2014) Prenatal immune activation induces
710 maturation-dependent alterations in the prefrontal GABAergic transcriptome.
711 Schizophr Bull 40:351-361.
712 Robinson S, Li Q, Dechant A, Cohen ML (2006) Neonatal loss of gamma-aminobutyric
713 acid pathway expression after human perinatal brain injury. J Neurosurg
714 104:396-408.
715 Salmaso N, Jablonska B, Scafidi J, Vaccarino FM, Gallo V (2014) Neurobiology of
716 premature brain injury. Nat Neurosci 17:341-346.
717 Salmaso N, Dominguez M, Kravitz J, Komitova M, Vaccarino FM, Schwartz ML (2015)
718 Contribution of maternal oxygenic state to the effects of chronic postnatal
719 hypoxia on mouse body and brain development. Neuroscience letters 604:12-17.
720 Salmaso N, Silbereis J, Komitova M, Mitchell P, Chapman K, Ment LR, Schwartz ML,
721 Vaccarino FM (2012) Environmental enrichment increases the GFAP+ stem cell
722 pool and reverses hypoxia-induced cognitive deficits in juvenile mice. The
723 Journal of neuroscience : the official journal of the Society for Neuroscience
724 32:8930-8939.
725 Samaco RC, Hogart A, LaSalle JM (2005) Epigenetic overlap in autism-spectrum
726 neurodevelopmental disorders: MECP2 deficiency causes reduced expression of
727 UBE3A and GABRB3. Hum Mol Genet 14:483-492.
728 Sanai N, Nguyen T, Ihrie RA, Mirzadeh Z, Tsai HH, Wong M, Gupta N, Berger MS,
729 Huang E, Garcia-Verdugo JM, Rowitch DH, Alvarez-Buylla A (2011) Corridors of
730 migrating neurons in the human brain and their decline during infancy. Nature
731 478:382-386.

732 Scafidi J, Hammond TR, Scafidi S, Ritter J, Jablonska B, Roncal M, Szigeti-Buck K,
733 Coman D, Huang Y, McCarter RJ, Jr., Hyder F, Horvath TL, Gallo V (2014)
734 Intranasal epidermal growth factor treatment rescues neonatal brain injury.
735 Nature 506:230-234.
736 Skorput AG, Gupta VP, Yeh PW, Yeh HH (2015) Persistent Interneuronopathy in the
737 Prefrontal Cortex of Young Adult Offspring Exposed to Ethanol In Utero. The
738 Journal of neuroscience : the official journal of the Society for Neuroscience
739 35:10977-10988.
740 Stevens HE, Su T, Yanagawa Y, Vaccarino FM (2013) Prenatal stress delays inhibitory
741 neuron progenitor migration in the developing neocortex.
742 Psychoneuroendocrinology 38:509-521.
743 Sugranyes G, Kyriakopoulos M, Corrigall R, Taylor E, Frangou S (2011) Autism
744 spectrum disorders and schizophrenia: meta-analysis of the neural correlates of
745 social cognition. PLoS One 6:e25322.
746 Takano T (2015) Interneuron Dysfunction in Syndromic Autism: Recent Advances. Dev
747 Neurosci 37:467-475.
748 Tooney PA, Chahl LA (2004) Neurons expressing calcium-binding proteins in the
749 prefrontal cortex in schizophrenia. Prog Neuropsychopharmacol Biol Psychiatry
750 28:273-278.
751 Torigoe M, Yamauchi K, Kimura T, Uemura Y, Murakami F (2016) Evidence That the
752 Laminar Fate of LGE/CGE-Derived Neocortical Interneurons Is Dependent on
753 Their Progenitor Domains. The Journal of neuroscience : the official journal of the
754 Society for Neuroscience 36:2044-2056.

755 Tremblay R, Lee S, Rudy B (2016) GABAergic Interneurons in the Neocortex: From
756 Cellular Properties to Circuits. Neuron 91:260-292.
757 Volk DW, Matsubara T, Li S, Sengupta EJ, Georgiev D, Minabe Y, Sampson A,
758 Hashimoto T, Lewis DA (2012) Deficits in transcriptional regulators of cortical
759 parvalbumin neurons in schizophrenia. Am J Psychiatry 169:1082-1091.
760 Voronova A, Yuzwa SA, Wang BS, Zahr S, Syal C, Wang J, Kaplan DR, Miller FD
761 (2017) Migrating Interneurons Secrete Fractalkine to Promote Oligodendrocyte
762 Formation in the Developing Mammalian Brain. Neuron 94:500-516.e509.
763 Yang Z, Ming GL, Song H (2011) Postnatal neurogenesis in the human forebrain: from
764 two migratory streams to dribbles. Cell Stem Cell 9:385-386.
765 Zhou Y, Huang X, Zhao T, Qiao M, Zhao X, Zhao M, Xu L, Zhao Y, Wu L, Wu K, Chen
766 R, Fan M, Zhu L (2017) Hypoxia augments LPS-induced inflammation and
767 triggers high altitude cerebral edema in mice. Brain Behav Immun 64:266-275.
768 Zonouzi M, Scafidi J, Li P, McEllin B, Edwards J, Dupree JL, Harvey L, Sun D, Hubner
769 CA, Cull-Candy SG, Farrant M, Gallo V (2015) GABAergic regulation of
770 cerebellar NG2 cell development is altered in perinatal white matter injury. Nat
771 Neurosci 18:674-682.

772

773 **Legends**

774 **Table 1.** List of donors (from NIH Neurobiobank, University of Maryland, Baltimore,
775 MD).

776

777 **Table 2.** Statistical analysis. ACC: anterior cingulate cortex, CP: cortical plate, LL:
778 lower layers, MIA-/CSH-: mice treated with saline and reared under normoxia,
779 MIA+/CSH-, mice subjected to maternal immune activation and reared under normoxia,
780 MIA-/CSH+: mice treated with saline and reared under chronic sublethal hypoxia and
781 (MIA+/CSH+): mice subjected to MIA and reared under CSH, MZ: marginal zone, ns:
782 non-significant, PL: Prelimbic areas, SVZ/VZ: subventricular/ventricular zone, SWM:
783 subcortical white matter, UL: upper layers.

784

785 **Figure 1.** Effect of prematurity on interneurons density in Brodmann Area 9 of male
786 infants. Illustration of **A**-**E**, Glutamate decarboxylase 65 and 67 (GAD65-67, green) **B**,
787 somatostatin (SST, red) **C**, calbindin (CLB, red) **D**, calretinin (CRT, red) and **E**,
788 neuropeptide Y (NPY, red) interneurons density. Scale bar = 20 µm. Quantification of
789 **A'**, GAD65-67 **B'**, SST **C'**, CLB **D'** CRT and **E'** NPY positive cells in the upper layers
790 (UL), lower layers (LL) and subcortical white matter (SWM) of the Brodmann Area 9 of
791 the frontal cortex of term and preterm male infants. BA9 of female infants are presented
792 on Figure 1-1. Interneuron-related protein expression and transcripts are presented in
793 Figures 1-2 and 1-3 respectively. Scatter dot plots represent the mean and individual
794 dispersion of seven to nine term (empty circles) and six to seven preterm infants (full
795 circles). * $p < 0.05$ (Two-Way ANOVAs were performed followed by Fisher's LSD tests
796 for post-hoc comparisons).

Figure 1-1. Effect of prematurity on interneurons density in Brodmann Area 9 of female infants. Quantification of **A**, GAD65-67 **B**, SST **C**, CLB **D,** CRT and **E,** NPY positive cells in the upper layers (UL), lower layers (LL) and subcortical white matter (SWM) of the Brodmann Area 9 of the frontal cortex of term and preterm female infants. Scatter dot plots represent the mean and individual dispersion of three term (empty circles) and four preterm infants (full circles). (Two-Way ANOVAs were performed followed by Fisher's LSD tests for post-hoc comparisons).

Figure 1-2. Effect of prematurity on interneuron-related protein expression in Brodmann Area 9 of male and female term and preterm infants. **A**, Representative blots of term (T) and preterm infants (PT); Quantification of protein expression of **B**, Glutamate decarboxylase 65 (GAD65); **C**, GAD67; **D**, somatostatin (SST); **E**, calbindin (CLB) and **F**, calretinin (CRT) in term (T, white bars) and preterm infants (PT, black bars). GAPDH was used for normalization. (Two-way ANOVA with Sidak's multiple comparisons).

Figure 1-3. Effect of prematurity on interneuron-related transcript expression in Brodmann Area 9 of male and female term and preterm infants. Quantification of mRNA levels of **A**, *gad1*; **B**, *gad2*; **C**, *sst*; **D**, *calb1*; **E**, *calb2* and **H**, *npy* in term (T, white bars) and preterm infants (PT, black bars). *tfrc* was used for normalization. * $p < 0.05$ (Two-way ANOVA with Sidak's multiple comparisons)

819 **Figure 2.** Effect of the multi-hit model on interneuron abundance and distribution in the
820 anterior cingulate cortex (ACC) and prelimbic area (PL) of the PFC at P30. Illustration of
821 **A**, cortical layer delineation with DAPI (blue), the density and laminar distribution of
822 GAD65 (green) overlaid with **B**, GAD67; **C**, somatostatin (SST) and **D**, calbindin (CLB)
823 (red) in the ACC and PL layers I, II/III, V and VI of mice treated with saline and reared
824 under normoxia or subjected to maternal immune activation (MIA, injected with
825 150µg/kg of LPS at E15.5 and E16.5) and reared under chronic sublethal hypoxia
826 (CSH). Scale bar = 100 µm. Five additional subtypes of interneuron were analyzed and
827 are presented in Figure 2-1. Quantification of interneurons **A'-D'**, in the ACC and **A''-**
828 **D''**, in the PL of mice treated with saline and reared under normoxia, subjected to with
829 MIA and reared under normoxia, treated with saline and reared under CSH and
830 subjected to MIA and reared under CSH. Layers densities are stacked and blue, red,
831 green and purple colors are assigned for layers I, II/III, V and VI respectively. Values
832 represent the mean (±SEM) from five to six animals out two pregnancies. * , +, •, #p <
833 0.05 (Kruskal-Wallis with Dunn's comparisons).
834

835 **Figure 2-1** Effect of the multi-hit model on interneuron abundance and distribution in the
836 anterior cingulate cortex (ACC) and prelimbic area (PL) of the PFC at P30. Illustration of
837 the density and laminar distribution of A-E, GAD65 (green) and overlaid with **A**,
838 parvalbumin (PV); **B**, vasoactive intestinal peptide (VIP); **C**, calretinin (CRT); **D**,
839 neuropeptide Y (NPY) and **E**, reelin (RLN) (red) in the ACC and PL layers I, II/III, V and
840 VI of mice treated with saline and reared under normoxia or subjected to maternal
841 immune activation (MIA, injected with 150µg/kg of LPS at E15.5 and E16.5) and reared
842 under chronic sublethal hypoxia (CSH). Scale bar = 100 µm. Quantification of

interneurons **A'-E'**, in the ACC and **A''-E''**, in the PL of mice treated with saline and reared under normoxia, subjected to with MIA and reared under normoxia, treated with saline and reared under CSH and subjected to MIA and reared under CSH. Layers densities are stacked and blue, red, green and purple colors are assigned for layers I, II/III, V and VI respectively. Values represent the mean (±SEM) from at five to six animals out of two pregnancies. * , +, •, #p < 0.05 (Kruskal-Wallis with Dunn's comparisons).

Figure 3. Effect of maternal immune activation (MIA) at E17.5 on interneuron progenitor's proliferation and fate. **A**, delineation of the sub-regions of the embryonic cortex with DAPI (blue); **A**' GAD65 density at E17.5 in the marginal zone (MZ), cortical plate (CP) and subventricular/ventricular zone (SVZ/VZ; green); Scale bar 100 µm. **A'**, Quantification of GAD65 positive cells in the MZ, CP, SVZ/VZ; **B**, GAD65 proliferation at E17.5 in the remaining caudal ganglionic eminence (CGE; density of GAD65 (green) and Ki67 (red)) Scale bar = 50 µm. Proliferation in the other ganglionic eminence areas is presented in Figure 3-1. Quantification of **B'**, GAD65; **B''**, Ki67 and **B***, GAD65 and Ki67 co-labeled cells density in the CGE; **C**, GAD65 cell fate in the cerebral cortex at E17.5 (GAD65 (green) and BrdU (red)) in mice subjected to saline or maternal immune activation (MIA, injected with 150µg/kg of LPS at E15.5 and E16.5) Scale bar = 50 µm. Quantification of **C'**, GAD65; **C''**, BrdU and **C***, GAD65 and BrdU positive cells in the cerebral cortex of mice treated with saline (white bars) and subjected to MIA (black bars). Apoptotic cell death and total neuronal densities are presented in Figures 3-2 and 3-3 respectively. Values represent the mean (±SEM) from five to six animals out two

866 pregnancies. A' * p < 0.05 (Two-way ANOVA with Sidak's multiple comparisons), B-C
867 *p<0.5, ** p < 0.01, ***p<001 (Mann-Whitney).

868

869 **Figure 3-1.** Effect of maternal immune activation (MIA) at E17.5 on Nkx2.1 interneurons
870 progenitors. Illustration of Nkx2.1 density **A**, in the medial ganglionic eminence (MGE);
871 **B**, in the preoptic area (POA), and **C** in the embryonic cortex i.e. marginal zone (MZ),
872 cortical plate (CP) and subventricular/ventricular zone (SVZ/VZ; green) of mice E17.5
873 subjected to saline or maternal immune activation (MIA, injected with 150µg/kg of LPS
874 at E15.5 and E16.5). Scale bar 100 µm. Quantification of nk2.1 positive cells **A**', in the
875 MGE; **B**', POA and **C**', cortex MZ, CP, SVZ/VZ positive cells in the cortex of mice
876 treated with saline (white bars) and subjected to MIA (black bars). Values represent the
877 mean (±SEM) from five to six animals out of two pregnancies. A'-B' (Mann-Whitney). C' *
878 p < 0.05 (Two-way ANOVA with Sidak's multiple comparisons).

879

880 **Figure 3-2.** Effect of maternal immune activation (MIA) at E17.5 on apoptotic cell death.
881 **A**, Illustration of cleaved-caspase 3 density, in the embryonic cortex of mice E17.5
882 subjected to saline or maternal immune activation (MIA, injected with 150µg/kg of LPS
883 at E15.5 and E16.5). Arrowheads highlight caspase-3 positive cells. The marginal zone
884 (MZ), cortical plate (CP) and subventricular/ventricular zone (SVZ/VZ) are added for
885 reference. Scale bar 50 µm. **B**, Quantification of cleaved-caspase 3 positive cells in the
886 cortex of E17.5 mice treated with saline (white bars) and subjected to MIA (black bars).
887 Values represent the mean (±SEM) from five to six animals out two pregnancies. * p <
888 0.05; *** p < 0.001 (Mann-Whitney).

889

890 **Figure 3-3.** Effect of maternal immune activation (MIA) at E17.5 on cell density. **A**,
891 Illustration of neuronal (with NeuN) and cellular (with DAPI) density, in the embryonic
892 cortex of mice E17.5 subjected to saline or maternal immune activation (MIA, injected
893 with 150µg/kg of LPS at E15.5 and E16.5). The marginal zone (MZ), cortical plate (CP)
894 and subventricular/ventricular zone (SVZ/VZ) are added for reference. Scale bar 50 µm.
895 Quantification of **B**, NeuN and **C**, DAPI positive cells in the cortex of E17.5 mice treated
896 with saline (white bars) and subjected to MIA (black bars). Values represent the mean
897 (±SEM) from five to six animals out of two pregnancies. ** $p < 0.01$ (Mann-Whitney).

898

899 **Table 3.** Effect of maternal immune activation (MIA) at E17.5 on the regulation of
900 interneurons fate determination and migration-related transcripts. Quantification of
901 mRNA levels in E17.5 embryos. Each value represents the mean (±SEM) from at least
902 five embryos out of at least two pregnancies. * $p < 0.05$; *** $p < 0.001$ (Mann-Whitney).

903

904 **Figure 4.** Effect of the multi-hit model on interneuron density and fate in the PFC at **A**,
905 P10 and **B**, P30. GAD65 cell fate in the cerebral cortex (GAD65 (green) and BrdU (red))
906 of A, mice treated with saline and reared under normoxia or subjected MIA and reared
907 under chronic sublethal hypoxia (CSH). Scale bar = 100 µm. Quantification of **A'**,
908 GAD65; **B'**, GAD65 and BrdU co-labeled cells density of P10; and **A''**, GAD65; **B''**,
909 GAD65 and BrdU co-labeled cells density at P30 in the PFC (the anterior cingulate
910 cortex (ACC) and prelimbic area (PL) are added for reference) with saline and reared

911 under normoxia, subjected to with MIA and reared under normoxia, treated with saline
912 and reared under CSH, subjected to MIA and reared under CSH. Values represent the
913 mean (±SEM) from five to six animals out two pregnancies. * $p < 0.05$ (Kruskal-Wallis
914 test with Dunn's multiple comparisons).

915

916 **Figure 5.** Effect of the multi-hit model on GAD65 positive cells density at E17.5, P10
917 and P30 in the prefrontal cortex of mice treated with saline and reared under normoxia,
918 subjected to with MIA and reared under normoxia, treated with saline and reared under
919 CSH, subjected to MIA and reared under CSH. Values represent the mean (±SEM) from
920 at least seven animals out of at least two pregnancies. * $p < 0.05$; *** $p < 0.001$ (Two-
921 way ANOVA, Tukey's multiple comparisons).

922

923 **Figure 6.** Effect of the multi-hit model on microglial density (Iba1) and activation (CD68)
924 in the PFC at **A**, E17.5 subjected to saline or maternal immune activation (MIA; injected
925 with 150µg/kg of LPS at E15.5 and E16.5); **B**, P10 and **C**, P30 mice treated with saline
926 and reared under normoxia or subjected to MIA and reared under chronic sublethal
927 hypoxia (CSH). Arrowheads highlight cells positive for Iba1 and CD68. Scale bar = 50
928 µm. Scale bar of inset = 15 µm. Quantification of Iba1 **A'**, at E17.5; **B'**, at P10; **C'**, at
929 P30 and CD68 **A''**, at E17.5; **B''**, at P10; **C''** positive cells of mice treated with saline
930 and reared under normoxia, subjected to with MIA and reared under normoxia, treated
931 with saline and reared under CSH, subjected to MIA and reared under CSH. Values
932 represent the mean (±SEM) from five to six animals out two pregnancies. A'-A'' * $p <$

933 0.05; ** p < 0.01 (Mann-Whitney). B'-C'' ** p < 0.01 (Kruskal-Wallis test with Dunn's
934 multiple comparisons).

935

936 **Figure 7.** Behavioral characterization. Assessment of working memory with
937 Spontaneous alternation in the Y-maze, mice were allowed to freely explore the maze
938 for 10 min. **A**, Alternation index. Reinvestigation in the Barnes maze, mice were allowed
939 to freely explore the maze for 10 min. **B**, Reinvestigation index. Assessment of learning
940 and reversal learning in the Water T-maze. Percentage of correct choice during **C**, the
941 learning phase (5 days) and **D**, the reversal phase of the test (4 days). Assessment of
942 social cognition in the three-chamber test. Percentage of time spent interacting between
943 **E**, a conspecific stranger (S1) versus an object; **F**, a novel (S2) and a familiar (S1)
944 conspecific; **G**, total time spent to interacting with conspecifics strangers of P30 mice
945 reared under normoxia, subjected to with maternal immune activation (MIA, injected
946 with 150µg/kg of LPS at E15.5 and E16.5) and reared under normoxia, treated with
947 saline and reared under chronic sublethal hypoxia (CSH), subjected to MIA and reared
948 under CSH. Complementary information is presented in Figure 7-1. Values represent
949 the mean (±SEM) from eight to twelve animals out of two pregnancies. A-B, E-G * p <
950 0.05; ** p < 0.01; ** p < 0.001 (One-way ANOVA with Holm-Sidak's multiple
951 comparisons), C-D * p < 0.05; ** p < 0.01; ** p < 0.001 (Two-way ANOVA with Tukey's
952 multiple comparisons).

953

954 **Figure 7-1.** Complementary behavioral characterization. Assessment of activity **A**, in
955 the Y-maze with the number of arm entries; **B**, in the Barnes maze with the number of

nose pokes and **C**, in the Open Field with the total distance traveled. Anxiety measurement in the Open Field **D**, Time spent in the border of the arena; **E**, Time spent in the center of the arena; **F**, Count of number of buried marbles in the marble burying test of P30 mice reared under normoxia, subjected to with maternal immune activation (MIA, injected with 150µg/kg of LPS at E15.5 and E16.5) and reared under normoxia, treated with saline and reared under chronic sublethal hypoxia (CSH), subjected to MIA and reared under CSH. Values represent the mean (±SEM) from eight to twelve animals out of two pregnancies. A-D, F non-significant (One-way ANOVA with Holm-Sidak's multiple comparisons), E non-significant (Kruskal-Wallis test with Dunn's multiple comparisons).

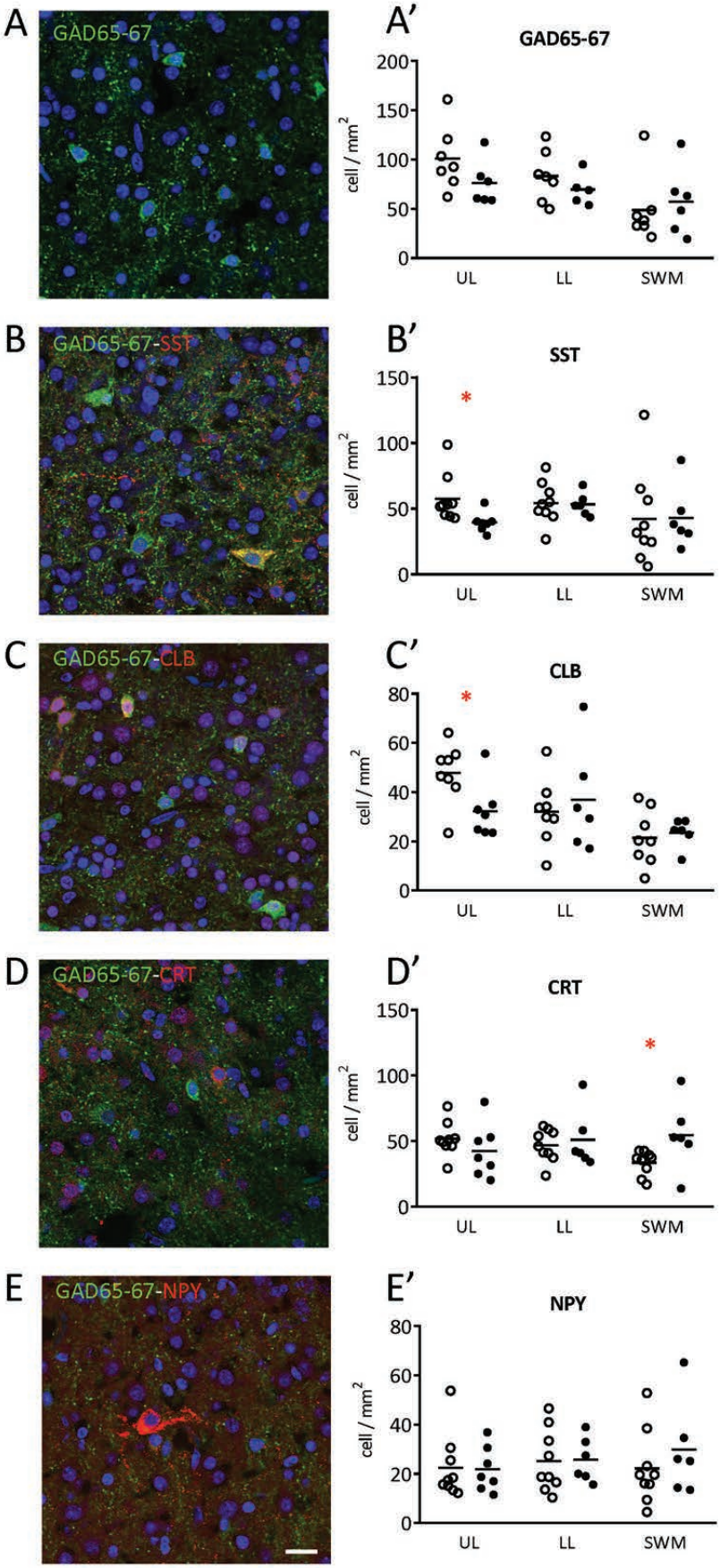

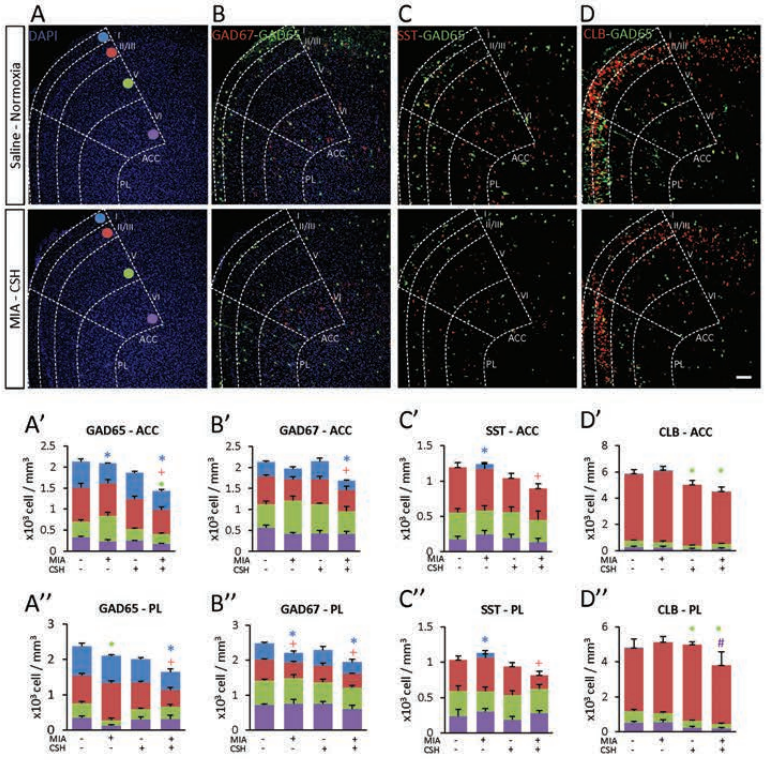

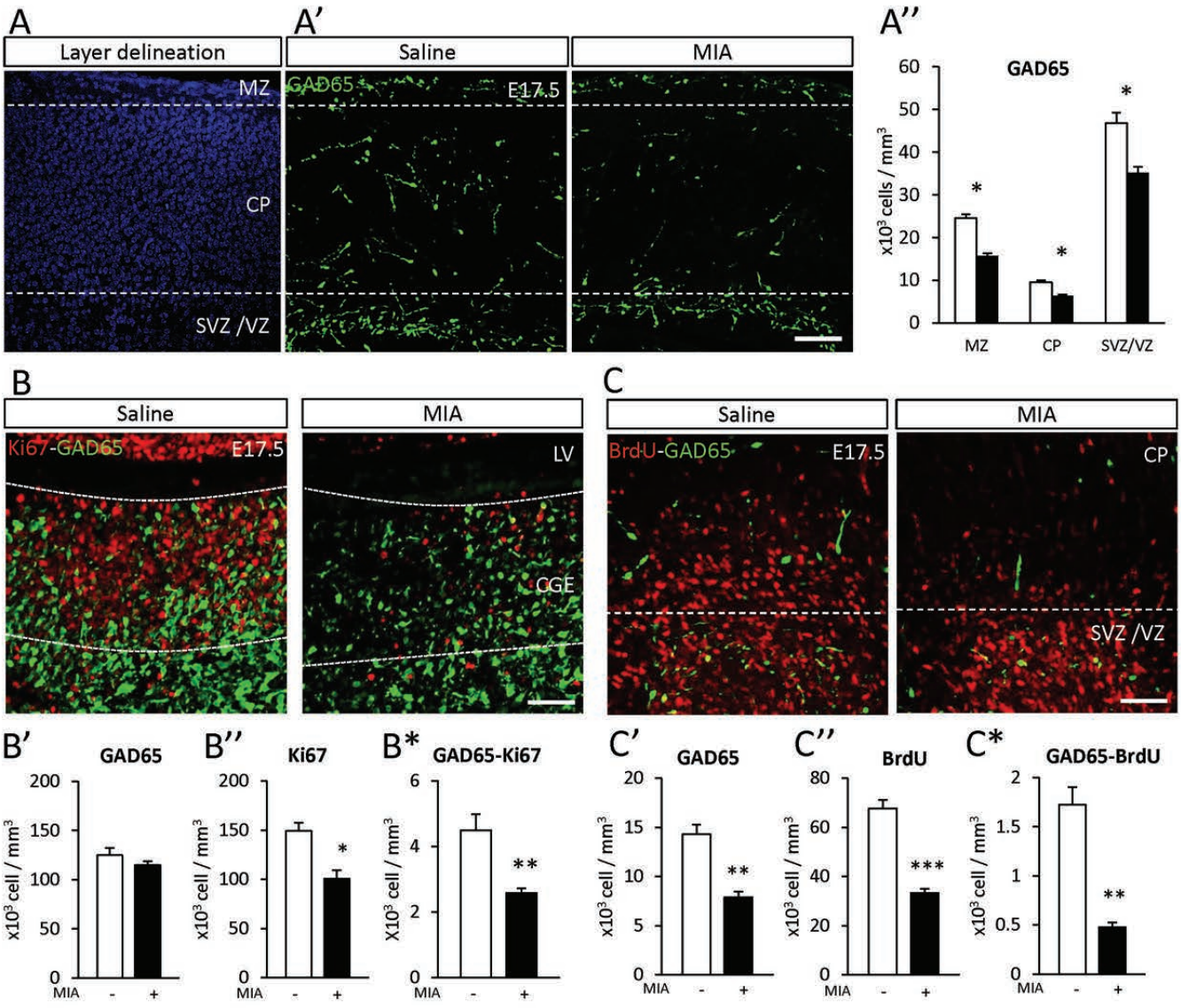

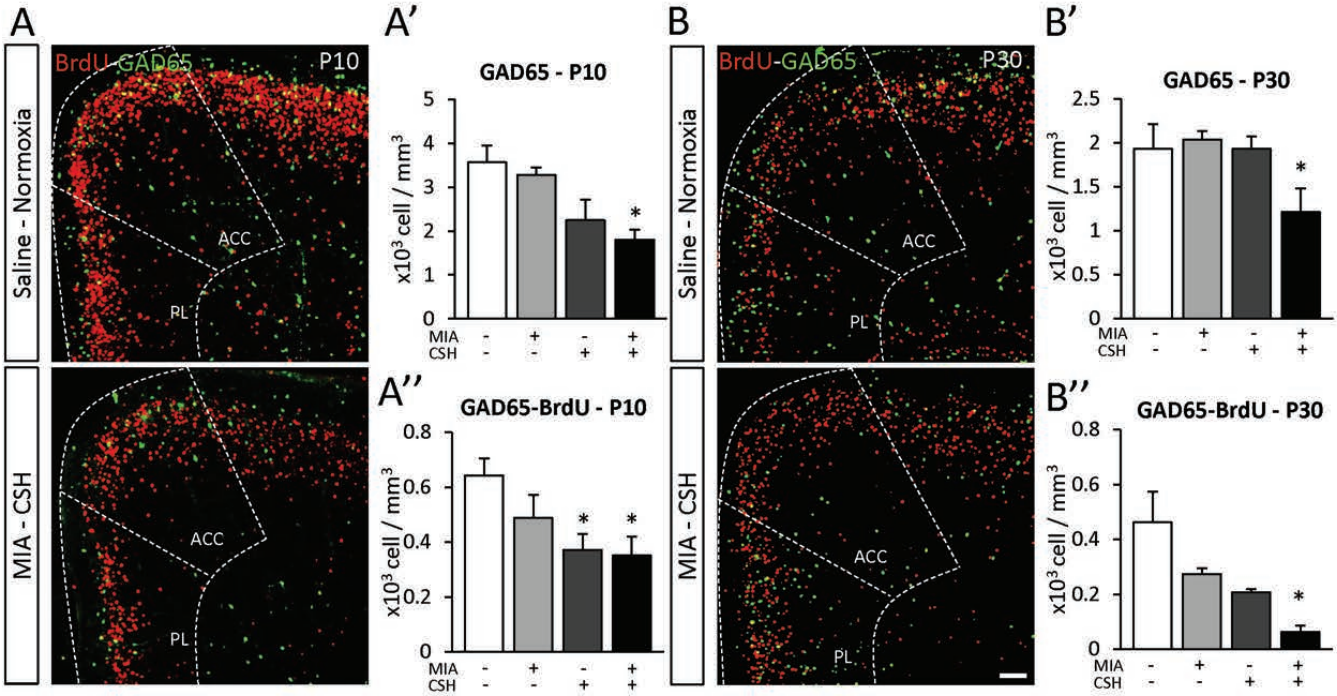

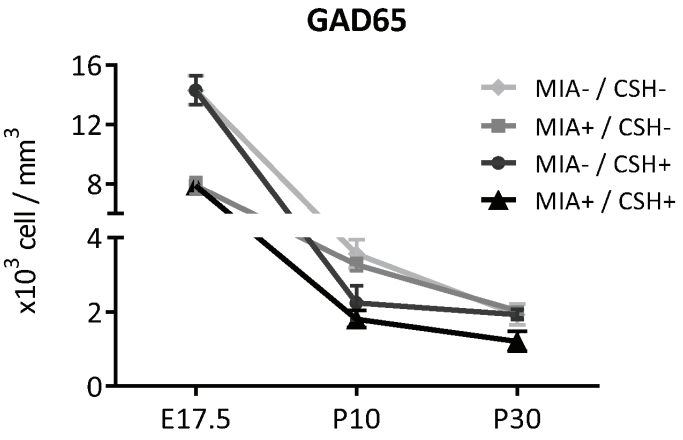

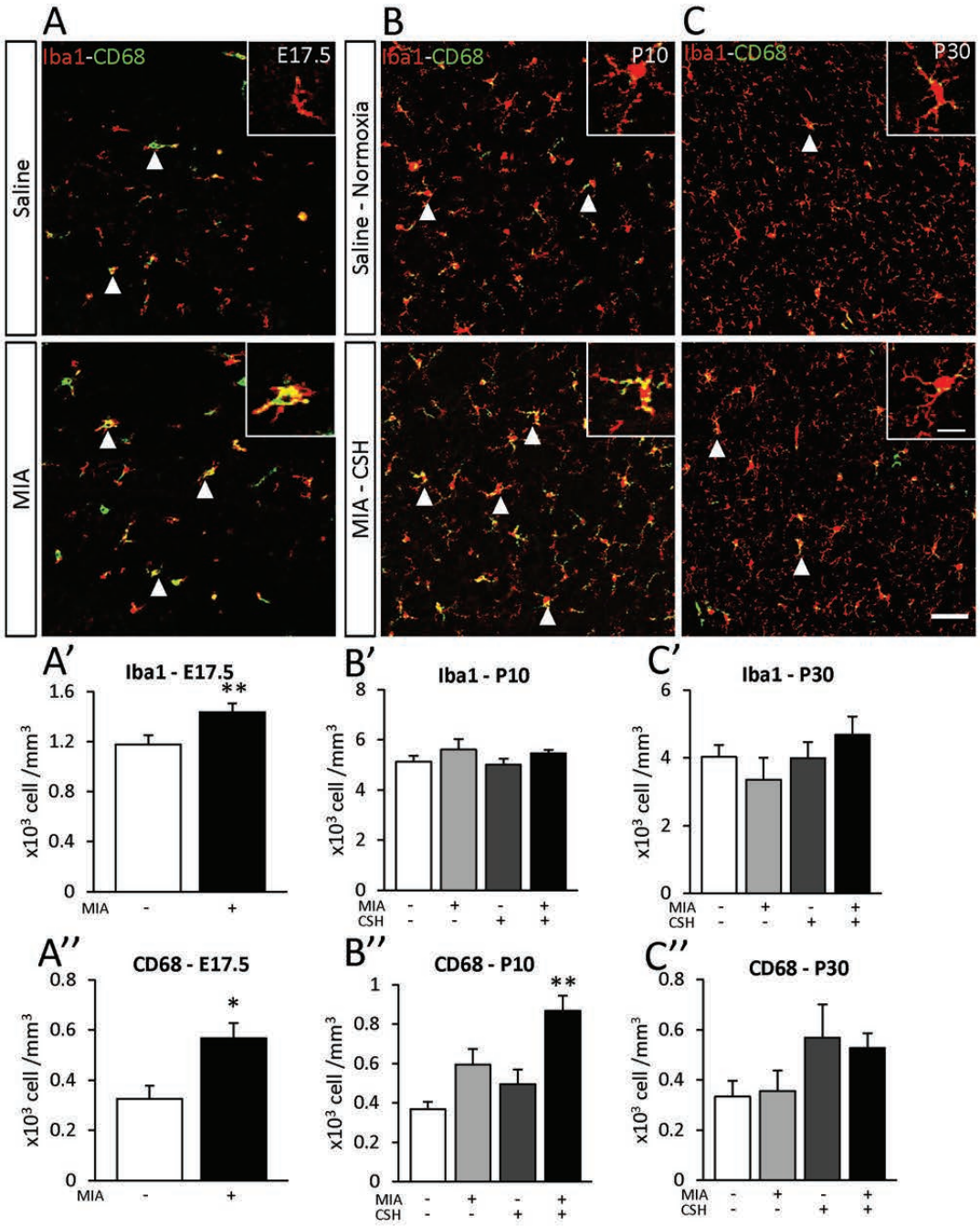

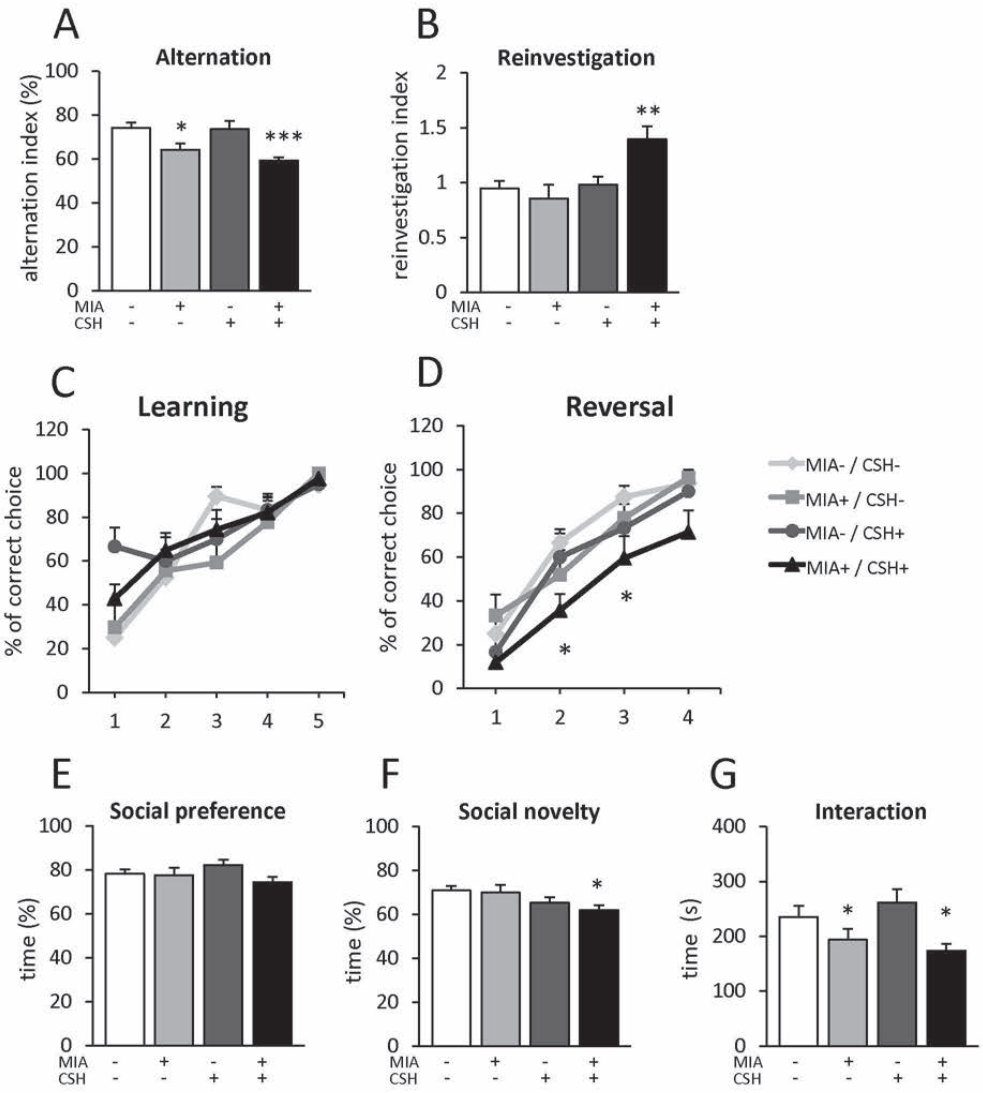

List of donors (from NIH Neurobiobank, University of Maryland, Baltimore, MD)

PRETERM INFANTS

Accession number	Sex	Gestational weeks	Absolute age (months)	Corrected age (months)	Cause of death
-1224	M	31	1.3	-1	Sudden Unexplained Death in Infancy
437	M	28	3.3	0.3	Sudden Unexplained Death in Infancy
934	M	27	4.5	1.3	Sudden Unexplained Death in Infancy
1325	F	25	6.1	2.3	Sudden Unexplained Death in Infancy
1487	F	29	2.1	-0.6	Prematurity with complications
4364	M	27	4.8	1.6	Prematurity, Pneumonia
4373	F	34	3.3	1.8	Methicillin susceptible Staphylococcus
4389	F	34	2.6	1.1	Positional Asphyxia
4416	F	26	4.7	1.2	Asphyxia, Prematurity
4417	M	28	2.4	-0.6	Undetermined, Hepatic Stenosis, Prematurity
5708	F	29	5.2	2.5	Viral syndrome with focal acute pneumonia
5716	M	29	3.2	0.5	Sudden Unexplained Death in Infancy

5754	M	33	5	3.2	Sudden Unexplained Death in Infancy
5843	M	34	3.3	1.8	Sudden Unexplained Death in Infancy

TERM CONTROL INFANTS

Accession number	Sex	Gestational weeks	Absolute age (months)	Corrected age (months)	Cause of death
4353	M	40	1.1	1.1	Positional asphyxia
4355	M	38	2.7	2.2	Prone Sleep position and excessive bedding
4375	F	40	0.1	0.1	Positional asphyxia
4381	F	40	3	3	Probable Aspshyxia
4383	F	40	2.5	2.5	Probable overlay
4391	M	40	0.9	0.9	Asphyxia due to co-sleeping
4402	M	39	2.2	2	Co-Sleeping
4412	M	40	2.2	2.2	Sudden Unexplained Infant Death
4414	F	37	1.3	0.5	Sudden Unexpected Infant Death with Co-sleeping
4420	M	40	2.1	2.1	Positional asphyxia
5658	M	38	1.4	0.9	Sudden Unexplained Death in Infancy
5761	F	38	1.1	0.6	Sudden Unexplained Death in Infancy

5886	M	40	1.5	1.5	Sudden Unexplained Death in Infancy

Statistical Analysis

Data set	Data structure	Type of test	Power
Fig1A	non-normal distribution	2way ANOVA, Uncorrected Fisher's LSD	UL: p=0.1337, LL: p=0.4334, SWM: p=0.5985
Fig1B	non-normal distribution	2way ANOVA, Uncorrected Fisher's LSD	UL: p=0.0425, LL: p=0.9257, SWM: p=0.9609
Fig1C	non-normal distribution	2way ANOVA, Uncorrected Fisher's LSD	UL: p=0.0278, LL: p=0.4931, SWM: p=0.7801
Fig1D	non-normal distribution	2way ANOVA, Uncorrected Fisher's LSD	UL: p=0.2880, LL: p=0.6393, SWM: p=0.0240
Fig1E	non-normal distribution	2way ANOVA, Uncorrected Fisher's LSD	UL: p=0.9257, LL: p=0.9397, SWM: p=0.2848
Fig1-1A	non-normal distribution	2way ANOVA, Uncorrected Fisher's LSD	UL: p=0.9265, LL: p=0.5300, SWM: p=0.4023
Fig1-1B	non-normal distribution	2way ANOVA, Uncorrected Fisher's LSD	UL: p=0.8052, LL: p=0.3294, SWM: p=0.8217
Fig1-1C	non-normal distribution	2way ANOVA, Uncorrected Fisher's LSD	UL: p=0.3699, LL: p=0.9644, SWM: p=0.9559

Fig1-1D	non-normal distribution	2way ANOVA, Uncorrected Fisher's LSD	UL: p=0.3370, LL: p=0.2271, SWM: p=0.3900
Fig1-1E	non-normal distribution	2way ANOVA, Uncorrected Fisher's LSD	UL: p=0.7681, LL: p=0.7659, SWM: p=0.6875
Fig1-2B	non-normal distribution	2way ANOVA, Sidak's multiple comparisons	male: p=0.9428, female: p=0.7868
Fig1-2C	non-normal distribution	2way ANOVA, Sidak's multiple comparisons	male: p=0.3033, female: p=0.8720
Fig1-2D	non-normal distribution	2way ANOVA, Sidak's multiple comparisons	male: p=0.9960, female: p=0.7304
Fig1-2E	non-normal distribution	2way ANOVA, Sidak's multiple comparisons	male: p=0.9940, female: p=0.9212
Fig1-2F	non-normal distribution	2way ANOVA, Sidak's multiple comparisons	male: p=0.8677, female: p=0.8035
Fig1-3A	non-normal distribution	2way ANOVA, Sidak's multiple comparisons	male: p=0.6754, female: p=0.9993
Fig1-3B	non-normal distribution	2way ANOVA, Sidak's multiple comparisons	male: p=0.0497, female: p=0.4501
Fig1-3C	non-normal	2way ANOVA, Sidak's multiple	male: p=0.7528, female: p=0.6561

	distribution	comparisons	
Fig1-3D	non-normal distribution	2way ANOVA, Sidak's multiple comparisons	male: p=0.0412, female: p=0.9986
Fig1-3E	non-normal distribution	2way ANOVA, Sidak's multiple comparisons	male: p=0.8936, female: p=0.9142
Fig1-3F	non-normal distribution	2way ANOVA, Sidak's multiple comparisons	male: p=0.9886, female: p=0.3146
Fig2A	non-normal distribution	Kruskal-Wallis, Dunn's multiple comparisons	ACC: layer I: MIA+/CSH- p<0.05, layer II/III MIA+/CSH+ p<0.05, PL: layer I: MIA+/CSH- p<0.05, layer II/III MIA+/CSH+ p<0.05
Fig2B	non-normal distribution	Kruskal-Wallis, Dunn's multiple comparisons	ACC: layer II/III: MIA+/CSH- p<0.05, MIA-/CSH+ p<0.05, MIA+/CSH+ p<0.05, PL: layer II/III: MIA+/CSH+ P<0.05
Fig2C	non-normal distribution	Kruskal-Wallis, Dunn's multiple comparisons	ACC: layer I: MIA+/CSH- p<0.05, MIA+/CSH+ p<0.05, layer II/III: MIA+/CSH+ p<0.05, layer V: MIA+/CSH+ p<0.05, PL : layer I: MIA+/CSH+ p<0.05, layer II/III: MIA+/CSH+ p<0.05, layer V: MIA+/CSH- p<0.05
Fig2D	non-normal distribution	Kruskal-Wallis, Dunn's multiple comparisons	ACC: layer I: MIA+/CSH+ p<0.05, layer II/III: MIA+/CSH+ p<0.05, PL: layer I: MIA+/CSH- p<0.05, MIA+/CSH+ p<0.05, layer II/III: MIA+/CSH- p<0.05, MIA+/CSH+ p<0.05, MIA+/CSH+ p<0.05

Fig2-1A	non-normal distribution	Kruskal-Wallis, Dunn's multiple comparisons	ACC: layer II/III: MIA+/CSH+ p<0.05, PL: layer II/III MIA+/CSH+ p<0.05
Fig2-1B	non-normal distribution	Kruskal-Wallis, Dunn's multiple comparisons	ACC: layer V MIA+/CSH- p<0.05, MIA+/CSH+ p<0.05, PL: layer II/III: MIA+/CSH- p<0.05, MIA+/CSH+ p<0.05, layer V: MIA+/CSH+ p<0.05
Fig2-1C	non-normal distribution	Kruskal-Wallis, Dunn's multiple comparisons	ACC: layer V MIA-/CSH+ p<0.05, MIA+/CSH+ p<0.05, PL: layer V MIA-/CSH+ p<0.05, MIA+/CSH+, layer VI: MIA-/CSH+ p<0.05
Fig2-1D	non-normal distribution	Kruskal-Wallis, Dunn's multiple comparisons	ACC: layer V and layer VI: MIA+/CSH- p<0.05, MIA-/CSH+ p<0.05, MIA+/CSH+ p<0.05, PL: layer II/III: MIA+/CSH- p<0.05, MIA-/CSH+ p<0.05, MIA+/CSH+ p<0.05, layer V: MIA+/CSH+ p<0.05
Fig2-1D	non-normal distribution	Kruskal-Wallis, Dunn's multiple comparisons	ACC: layer I: MIA-/CSH+ p<0.05, PL: ns
Fig3A	non-normal distribution	2way ANOVA, Sidak's multiple comparisons	MZ: p<0.05, CP: p=<0.05, SVZ/VZ p<0.05
Fig3B	non-normal distribution	Mann-Whitney	gad65+: p=0.3333, ki67+: p=0.0381, gad65+/ki67+: p=0.0095
Fig3C	non-normal distribution	Mann-Whitney	gad65+: p=0.0012, brdu+: p<0.001, gad65+/brdu+: p=0.0012

Fig3-1A	non-normal distribution	Mann-Whitney	ns
Fig3-1B	non-normal distribution	Mann-Whitney	ns
Fig3-1C	non-normal distribution	2way ANOVA, Sidak's multiple comparisons	MZ: p=0.714, CP: p=0.04521, SVZ/VZ: p=0.1657
Fig3-2	non-normal distribution	Mann-Whitney	p= 0.0688
Fig3-3B	non-normal distribution	Mann-Whitney	p=0.0047
Fig3-3C	non-normal distribution	Mann-Whitney	p=0.0315
Fig4A	non-normal distribution	Kruskal-Wallis, Dunn's multiple comparisons	gad65+: MIA+/CSH+ p<0.05;
Fig4B	non-normal distribution	Kruskal-Wallis, Dunn's multiple comparisons	gad65+: MIA+/CSH+ p<0.05; gad65+/brdu+: MIA+/CSH+ p<0.05
Fig5	non-normal distribution	2way ANOVA, Tukey's multiple comparisons	e17.5: MIA+/CSH- p<0.001, P10: MIA+/CSH+ p<0.05, P30: MIA+/CSH+ p<0.05

Fig6A	non-normal distribution	Mann-Whitney	iba1+: p=0.0067, cd68+: p=0.0163
Fig6B	non-normal distribution	Kruskal-Wallis, Dunn's multiple comparisons	iba1+: ns, cd68+: MIA+/CSH+ p<0.01
Fig6C	non-normal distribution	Kruskal-Wallis, Dunn's multiple comparisons	iba1+: ns, cd68+: ns
Fig7A	normal distribution	1way ANOVA, Holm-Sidak's multiple comparisons	MIA+/CSH- p<0.05, MIA+/CSH+ p<0.001
Fig7B	normal distribution	1way ANOVA, Holm-Sidak's multiple comparisons	MIA+/CSH+ p<0.01
Fig7C	normal distribution	2way ANOVA, Tukey's multiple comparisons	ns
Fig7D	normal distribution	2way ANOVA, Tukey's multiple comparisons	d2: MIA+/CSH+ p<0.05, d3: MIA+/CSH+ p<0.05
Fig7E	normal distribution	1way ANOVA, Holm-Sidak's multiple comparisons	ns
Fig7F	normal distribution	1way ANOVA, Holm-Sidak's multiple comparisons	MIA+/CSH+ p<0.05
Fig7G	normal	1way ANOVA, Holm-Sidak's multiple	MIA+/CSH- p<0.05, MIA+/CSH+ p<0.05

	distribution	comparisons	
Fig7-1A	normal distribution	1way ANOVA, Holm-Sidak's multiple comparisons	ns
Fig7-1B	normal distribution	1way ANOVA, Holm-Sidak's multiple comparisons	ns
Fig7-1C	normal distribution	1way ANOVA, Holm-Sidak's multiple comparisons	ns
Fig7-1D	normal distribution	1way ANOVA, Holm-Sidak's multiple comparisons	ns
Fig7-1E	non-normal distribution	Kruskal-Wallis, Dunn's multiple comparisons	ns
Fig7-1F	normal distribution	1way ANOVA, Holm-Sidak's multiple comparisons	ns

Effect of maternal immune activation (MIA) at E17.5 on the regulation of interneurons fate determination and migration-related transcripts.

Gene symbol	Gene name	Fold change	SEM	Significance
gad1 (gad67)	glutamate decarboxylase 1	1.11	0.07	
gad2 (gad65)	glutamate decarboxylase 2	1.57	0.07	*
nkx2.1	NK2 homeobox 1	2.42	0.29	***
ascl1 (mash1)	achaete-scute family bHLH transcription factor 1	1.39	0.09	
pax6	paired box 6	1.02	0.16	
lhx6	LIM homeobox protein 6	1.92	0.19	*
ki67	antigen identified by monoclonal antibody Ki67	1.62	0.08	*
dlx1	distal-less homeobox 1	1.51	0.07	*
dlx2	distal-less homeobox 2	1.12	0.17	
dlx5	distal-less homeobox 5	2.76	0.53	***
dlx6	distal-less homeobox 6	0.98	0.10	